Alma Mater Studiorum · Università di Bologna

Scuola di Scienze
Dipartimento di Fisica e Astronomia
Corso di Laurea in Fisica

Constraining a top-philic fifth force studying toponium spectrum

Relatore:
Prof. Fabio Maltoni

Presentata da:
Simone Tentori

Anno Accademico 2019/2020

Sommario

In questa tesi viene analizzato un possibile mesone formato da un quark top e un quark antitop chiamato toponio usando la meccanica quantistica. Sono determinati i primi 6 livelli energetici degli orbitali S,P,D e F, la velocità e il raggio caratteristico del primo stato legato e lo splitting nei livelli S dovuto all'interazione spin-spin. Si ipotizza inoltre l'esistenza di una forza sconosciuta oltre il Modello Standard, mediata da una particela scalare, e se ne studia l'effetto sui livelli energetici determinati in precedenza. Data l'esistenza di questa forza si ha una diminuzione del tempo di formazione del toponio rispetto a quello previsto dal Modello Standard, si procederà quindi a stimare sommariamente l'intensità minima necessaria per questa forza affinché sia possibile la formazione di stati legati.

Abstract

In this thesis is analyzed, using quantum mechanics, a possible meson formed by a top antitop quark pair, called toponium. We have determined the first 6 energy levels of the S, P, D and F orbitals, the velocity and the characteristic radius of the first bound state and the energy splitting in the S levels due to the spin-spin interaction. Furthermore, we hypothesize the existence of an unknown force, mediated by a scalar particle, beyond the standard model and study the effect of this force on the previously calculated energy levels. It is possible to determine the minimum intensity of this force for which toponium formation time becomes smaller than its decay time, allowing the formations of top-antitop bounded states, otherwise forbidden by Standard Model.

Contents

List of Figures

List of Tables

Introduction

In the Standard Model framework top quark do not hadronize, the formation of the top related quarkonium, called toponium, is so inhibited. This is no longer true if we consider the existence of an unknown attractive top-philic force carried by an unknown scalar particle. The purpose of this thesis is to constrain this force, studying which intensity should have to allow toponium formation.

It is possible to treat quarkonia in the quantum mechanic framework using the Cornell potential, formed by a linear and a coulombic part.

The first chapter is dedicated to the exposition of some quantum mechanics results and theorem that will be useful in the following chapters.

In chapter two are analyzed two possible ways to solve the 1D Schrödinger problem, with particular attention to the radial case. WKB approximation is presented for the S states, while Numerov's algorithm is introduced solve numerically the Schrödinger equation in spherical coordinates.

In chapter three we try to determine Cornell potential parameters fitting Bottomonium spectrum, chosen for the abundance of experimental data, particular attention is dedicated to understand what is the right energy scale of the problem, from which α_s should depends.

Finally in the fourth chapter we modify Cornell potential adding a Yukawa one, and we study what happen to energy levels depending on the mass of the scalar particle, and the intensity of the interaction.

Chapter 1

Quantum Mechanics tools

The correct way to study the strong interactions is quantum chromodynamics (QCD), however for heavy quarkonia other methods were developed.

Light quarks move at relativistic speed in mesons but for heavy quarks (charm, bottom, top) the situation is different and, because of their large masses, a non-relativistic treatment can be performed using quantum mechanics.

In order to build an effective potential suitable for representing the interactions between quarks, two key phenomena need to be considered: the gluon exchange and the quarks confinement. These two features are embodied in the Cornell potential[1][2]:

$$V(r) = -\frac{4}{3}\frac{\alpha_s}{r} + \frac{r}{a^2} \tag{1.0.1}$$

in which the Coulomb part represents the short-range quark-antiquark force due to gluon exchange, and the linear part is capable of confining quarks permanently.

The parameter α_s is the strong coupling constant, depending on the quark mass, the parameter a should not depend on the quark flavour.

In this chapter we will briefly resume some quantum mechanics results.

1.1 Schrödinger equation

In order to get the wave function $\psi(\vec{x}, t)$ of a particle subjected to a potential U, we need to solve the Schrödinger equation:

$$-\frac{\hbar^2}{2m}\nabla^2\psi(\vec{x}, t) + U(\vec{x}, t)\psi(\vec{x}, t) = i\hbar\frac{\partial\psi(\vec{x}, t)}{\partial t} \tag{1.1.1}$$

If U is independent of t it is possible to solve eq. (1.1.1) using separation of variables, writing $\psi(\vec{x},t) = \phi(\vec{x})\tau(t)$. In this case eq. (1.1.1) becomes:

$$-\frac{\hbar^2}{2m}\tau(t)\nabla^2\phi(\vec{x}) + U(x)\tau(t)\phi(\vec{x}) = i\hbar\phi(\vec{x})\frac{\partial\tau(t)}{\partial t}$$

and dividing by $\phi(\vec{x})\tau(t)$

$$-\frac{\hbar^2}{2m}\frac{1}{\phi(\vec{x})}\nabla^2\phi(\vec{x}) + U(x) = i\hbar\frac{1}{\tau(t)}\frac{\partial\tau(t)}{\partial t} \tag{1.1.2}$$

The left member of eq. (1.1.2) depends on t alone and the right member on $\vec{x}$ alone, the only way in which these two could be equal is if they are constant.

For this reason we put:

$$i\hbar\frac{1}{\tau(t)}\frac{\partial\tau(t)}{\partial t} = E \tag{1.1.3}$$

that gives us:

$$\tau(t) = e^{-\frac{iE}{\hbar}(t-t_0)} \tag{1.1.4}$$

We have obtained the time-independent Schrödinger equation:

$$\nabla^2\phi(\vec{x}) + \frac{2m}{\hbar^2}\big(E - V(\vec{x})\big)\phi(\vec{x}) = 0 \tag{1.1.5}$$

If $\phi(\vec{x})$ is a solution of the Schrödinger equation with domain D, the following conditions must hold:

- $\phi(\vec{x})$ is not identically zero in D;
- $\phi(\vec{x})$ must be zero in ∂D;
- $\lim_{|\vec{x}|\to\infty} |\phi(\vec{x})| \leq C$
- $\phi(\vec{x})$ and $\nabla\phi(\vec{x})$ are continuous in D.

1.1.1 One dimensional Schrödinger equation

Some useful results are valid for the one dimensional case of the time-independent Schrödinger equation:

$$\frac{d^2}{dx^2}\phi(x) + \frac{2m}{\hbar^2}\big(E - V(x)\big)\phi(\vec{x}) = 0 \tag{1.1.6}$$

Some useful information about the energy spectrum could be obtained from the form of the potential $U(x)$: let's call $U_+ = \lim_{x\to+\infty} U(x)$, $U_- = \lim_{x\to-\infty} U(x)$, $U_< = \min(U_+, U_-)$ and $U_> = \max(U_+, U_-)$. The entire energy spectrum is contained in the energy range $E > \min(U(x))$, that could be divided in three parts:

- $\min(U(x)) < E < U_<$, in this interval the energy spectrum is discrete and non degenerate, the eigenfunctions are normalizable;
- $U_< < E < U_>$, in this interval the energy spectrum is continuous and non degenerate, the eigenfunctions are not normalizable;
- $E > U_>$, in this interval the energy spectrum is continuous and doubly degenerate, the eigenfunctions are not normalizable.

These results can be obtained studying the asymptotic behaviour of the solutions of eq. (1.1.6).

It is possible to label the energy eigenvalues of the discrete part of the energy spectrum, starting from the ground state E_1, in such a way that $E_n < E_{n+1}$.

Nodes theorem: any eigenfunctions ϕ_n associated to the energy eigenvalue E_n has exactly $n-1$ nodes.

x_0 is a node of the eigenfunction ϕ_n with domain D, if $x_0 \in Int(D)$ and $\phi_n(x_0) = 0$.

1.1.2 Schrödinger equation with a central potential

The potentials used to study quarkonia from a quantum mechanics point of view are central: $U(r, \theta, \varphi) = U(r)$.

Solving the Schrödinger equation with this type of potential is easier if it is rewritten in spherical coordinates:

$$\frac{\partial^2\phi}{\partial r^2}+\frac{2}{r}\frac{\partial\phi}{\partial r}+\frac{1}{r^2\sin^2\theta}\left[\sin\theta\frac{\partial}{\partial\theta}(\sin\theta\frac{\partial\phi}{\partial\theta})+\frac{\partial^2\phi}{\partial\varphi^2}\right]+\frac{2m}{\hbar^2}(E-U(r))\phi = 0 \quad (1.1.7)$$

In eq. (1.1.7) there are no mixed derivatives, we can formulate an ansatz for the solution: $\phi(r, \theta, \varphi) = R(r)Y(\theta, \varphi)$. Using this ansatz eq. (1.1.7) becomes:

$$\left[\frac{1}{R}\frac{d}{dr}\left(r^2\frac{dR}{dr}\right)+\frac{2mr^2}{\hbar^2}(E-U)\right]+ \\ +\frac{1}{Y}\left[\frac{1}{\sin\theta}\frac{d}{d\theta}\left(\sin\theta\frac{dY}{d\theta}\right)+\frac{1}{\sin^2\theta}\left(\frac{d^2Y}{d\varphi^2}\right)\right] = 0 \quad (1.1.8)$$

The term in the first brackets of eq. (1.1.8) depends on r alone and the term in the second bracket depends on θ, ϕ alone, the only way in which their sum

can be zero is if they are both constants.

$$\left[\frac{1}{R}\frac{d}{dr}\left(r^2\frac{dR}{dr}\right)+\frac{2mr^2}{\hbar^2}(E-U)\right]=l(l+1) \tag{1.1.9}$$

$$\frac{1}{Y}\left[\frac{1}{\sin\theta}\frac{d}{d\theta}\left(\sin\theta\frac{dY}{d\theta}\right)+\frac{1}{\sin^2\theta}\left(\frac{d^2Y}{d\varphi^2}\right)\right]=-l(l+1) \tag{1.1.10}$$

Eq. (1.1.10) can be solved using variable separations $Y(\theta,\varphi)=\Theta(\theta)\Phi(\varphi)$. Performing the same reasoning made before, we can write two separate equations:

$$\frac{1}{\Phi}\frac{d^2\Phi}{d\varphi^2}=-m^2 \tag{1.1.11}$$

$$\frac{1}{\Theta}\left[\sin\theta\frac{d}{d\theta}\left(\sin\theta\frac{d\Theta}{d\theta}\right)\right]+l(l+1)\sin^2\theta=m^2 \tag{1.1.12}$$

The eq. (1.1.11) solutions are trivial:

$$\Phi(\varphi)=c_+e^{im\varphi}+c_-e^{-im\varphi}\quad\text{if } m\neq 0 \tag{1.1.13}$$

$$\Phi(\varphi)=a\varphi+b\quad\text{if } m=0 \tag{1.1.14}$$

We know that $\Phi(\varphi)=\Phi(\varphi+2n\pi)$, so m must assume only integer values and the constant a in solution (1.1.14) must be equal to zero. Moreover if we change the sign of m eq. (1.1.11) remain the same, therefore we find that $c_+=c_-$. The general set of normalized solutions is:

$$\Phi(\varphi)=\frac{e^{im\varphi}}{\sqrt{2\pi}}\quad\text{with } m\in\mathbb{Z} \tag{1.1.15}$$

The solution of equation (1.1.12) it is not easy, with the substitution $u=\cos\theta$, we find:

$$(1-u^2)\frac{d^2\Theta}{du^2}-2u\frac{d\Theta}{du}+\left[l(l+1)-\frac{m^2}{1-u^2}\right]u=0 \tag{1.1.16}$$

this is an instance of the associated Legendre equation, the solutions diverge in $u=\pm1$ except if l is an integer equal or greater than zero and $|m|\leq l$. The solution of eq. (1.1.16) are the associated Legendre polynomials P_l^m:

$$P_l^m(u)=\frac{1}{2^l l!}(1-u^2)^{\frac{m}{2}}\frac{d^{m+l}}{du^{m+l}}(u^2-1)^l \tag{1.1.17}$$

Finally we find the complete solution of eq. (1.1.10), the so-called spherical harmonics:

$$Y(\theta,\varphi)_{l,m} = (-1)^m \left[\frac{2l+1}{4\pi}\frac{(l-m)!}{(l+m)!}\right]^{\frac{1}{2}} P_l^m(\cos\theta)e^{im\varphi} \tag{1.1.18}$$

Rewriting eq. (1.1.9) with the substitution $R(r) = \frac{\chi(r)}{r}$ we obtain:

$$\frac{d^2\chi}{dr^2} + \frac{2m}{\hbar^2}\left(E - U(r) - \frac{\hbar^2}{2m}\frac{l(l+1)}{r^2}\right)\chi = 0 \tag{1.1.19}$$

Eq. (1.1.19) is called Schrödinger radial equation and their solutions $\chi(r)$ radial wave functions. We can call:

$$V_{eff}(r) = U(r) + \frac{\hbar^2}{2m}\frac{l(l+1)}{r^2} \tag{1.1.20}$$

in this way eq. (1.1.19) has the same form of eq. (1.1.6) and we can apply to the radial problem the results for the one dimensional problem stated in the previous section. There is a further condition: if the short distance centrifugal dominance is valid, i.e. if $\lim_{r\to 0} r^2U(r) = 0$, then $\chi(0) = 0$. For two particle systems we substitute the mass m with the reduced mass mu in the Schrödinger equation, in order to find the energy eigenvalues.

1.1.3 Rescaling Schrödinger equation

We will now consider potentials of the form:

$$V(r) = \lambda r^\nu \tag{1.1.21}$$

for which the radial Schrödinger equation is:

$$\frac{d^2\chi}{dr^2} + \frac{2\mu}{\hbar^2}\left(E - \lambda r^\nu - \frac{\hbar^2}{2\mu}\frac{l(l+1)}{r^2}\right)\chi = 0 \tag{1.1.22}$$

we want to cast it in dimensionless form. The parameter λ, with $c = 1$, is in unit of:

$$[\lambda] = [\hbar^{-\nu}\mu^{\nu+1}] \tag{1.1.23}$$

the scaled measure of length ρ is:

$$\rho = \left(\frac{\hbar^2}{2\mu\,|\lambda|}\right)^p r \tag{1.1.24}$$

With this substitution eq. (1.1.22) becomes:

$$\frac{d^2\chi}{d\rho^2} + \left[\frac{2\mu}{\hbar^2}\left(\frac{2\mu\,|\lambda|}{\hbar^2}\right)^{2p} E - \left(\frac{2\mu\,|\lambda|}{\hbar^2}\right)^{p(2+\nu)+1} \mathrm{sign}(\lambda)\rho^\nu - \frac{l(l+1)}{\rho^2}\right]\chi = 0 \tag{1.1.25}$$

To eliminate the explicit dependence from mass and λ we set:

$$p = -\frac{1}{2+\nu} \tag{1.1.26}$$

$$\epsilon = \frac{2\mu}{\hbar^2}\left(\frac{2\mu\,|\lambda|}{\hbar^2}\right)^{2p} E \tag{1.1.27}$$

in this way we obtain the dimensionless form of the Schrödinger equation (1.1.22):

$$\frac{d^2\chi}{d\rho^2} + \left[\epsilon - \mathrm{sign}(\lambda)\rho^\nu - \frac{l(l+1)}{\rho^2}\right] = 0 \tag{1.1.28}$$

From eq. (1.1.27) we obtain how the level spacings depend on mass and coupling strength:

$$\Delta E \propto \left(\frac{2\mu}{\hbar^2}\right)^{-\frac{\nu}{2+\nu}} |\lambda|^{\frac{2}{2+\nu}} \tag{1.1.29}$$

From eq. (1.1.29), for the Coulomb potential we find the well-known result that the Rydberg constant is proportional to $\mu\,|\lambda|^2$. For the linear potential, as we will see also solving the Schrödinger equation later, the energy level spacing scale as: $\left(\frac{|\lambda|^2}{\mu}\right)^{\frac{1}{3}}$.

1.1.4 Useful Theorems

The virial theorem states that:

$$\langle T\rangle = E - \langle V\rangle = \left\langle \frac{r}{2}\frac{dV}{dr}\right\rangle \tag{1.1.30}$$

for a potential of type (1.1.21) we find useful formulas to connect directly $\langle T\rangle$ and $\langle V\rangle$ with E:

$$\langle V\rangle = \frac{2}{2+\nu}E \tag{1.1.31}$$

$$\langle T\rangle = \frac{\nu}{2+\nu}E \tag{1.1.32}$$

Another useful relation is the one that connects the s-wave functions at the origin and the gradient of the potential:

$$|\psi(0)|^2 = \frac{m}{2\pi\hbar^2}\left\langle \frac{dV}{dr}\right\rangle \tag{1.1.33}$$

Chapter 2

Schrödigner equation solving strategies

2.1 WKB approximation

For a Cornell-like potential, the Schrödinger's equation has no simple results that can be calculated analytically, therefore, in order to find the energy eigenvalues, we have to use numerical methods or approximate methods.

The WKB approximation [3] was formulated in 1926 by Wentzel-Kramers and Brillouin who found it independently, even if the first formulation was made in 1923 by the mathematician Jeffreys.

Let's consider a one-dimensional Schrödinger equation, we call

$$p(x)^2 = 2m\big(E - V(x)\big) \tag{2.1.1}$$

the classical momentum, and we remember the general form of a wave function:

$$\psi(x,t) = \sqrt{\rho(x,t)}\exp\left(\frac{i\mathcal{S}(x,t)}{\hbar}\right) = \exp\left(\frac{iS(x,t)}{\hbar}\right) \tag{2.1.2}$$

in which, to obtain the last result, we have written ρ as a complex exponential. We are interested in stationary states, so we can use the time independent Schrödinger equation, putting the expression of $\psi(x,t)$ from eq. (2.1.2) in (1.1.6) and using (2.1.1) we obtain:

$$\begin{aligned} -\hbar^2\frac{d^2}{dx^2}(e^{\frac{iS(x)}{\hbar}}) = -\hbar^2\left(\frac{i}{\hbar}S(x)'' + (\frac{i}{\hbar}S(x)')^2\right)e^{\frac{iS(x)}{\hbar}} = p(x)^2 e^{\frac{iS(x)}{\hbar}} \\ S'(x)^2 - i\hbar S(x)''(x) = p(x)^2 \end{aligned} \tag{2.1.3}$$

The differential equation (2.1.3) obtained is non-linear, so it could seem that we have complicated the original one, but now comes the WKB approximation: if we have a slowly varying potential $i\hbar S(x)''$ will be very small (if we

take a constant potential $S(x)'' = 0$). This is equivalent to consider $\hbar$ a small parameter[1], so we can expand S in unit of $\hbar$ as:

$$S(x) = S_0(x) + \hbar S_1(x) + \hbar^2 S_2(x) + \mathcal{O}(\hbar^3). \tag{2.1.4}$$

and inserting this result in (2.1.3) we find:

$$\big(S_0'(x)+\hbar S_1(x)+\mathcal{O}(\hbar^2)\big)^2 - p(x)^2 - i\hbar\big(S_0''(x)+\hbar S_1''(x)+\mathcal{O}(\hbar^2)\big) = 0. \tag{2.1.5}$$

Now we can stop the expansion at the desired order, if we choose the first one 2.1.5 reads:

$$[S_0'(x)^2 - p(x)^2] + \hbar[2S_0'(x)S_1'(x) - iS_0''(x)] + \mathcal{O}(\hbar^2) = 0. \tag{2.1.6}$$

In order to obtain zero, each coefficient of $\hbar$ powers must be zero. We obtain two conditions:

$$S_0'(x)^2 - p(x)^2 = 0 \tag{2.1.7a}$$

$$S_1'(x) = \frac{i}{2}\frac{S_0''(x)}{S_0'(x)} \tag{2.1.7b}$$

From (2.1.7a) we easily obtain $S_0'(x) = \pm p(x)$ and:

$$S_0(x) = \pm \int_{x_0}^{x} p(x')dx' \tag{2.1.8}$$

with x_0 a constant to be adjusted. Inserting the result of (2.1.7a) in (2.1.7b) we obtain:

$$S_1'(x) = \frac{i}{2}\frac{\pm p'(x)}{\pm p(x)} \tag{2.1.9}$$

that can be integrated to give:

$$S_1(x) = \frac{i}{2}\ln p(x) + C. \tag{2.1.10}$$

We can now use (2.1.9) and (2.1.10) to obtain the approximate form of the wave function:

$$\psi(x) = e^{\frac{i}{\hbar}[S_0(x)+\hbar S_1(x)]} = e^{\frac{i}{\hbar}S_0(x)}e^{\frac{i}{2}\ln p(x)+C} = \frac{K}{\sqrt{p(x)}}e^{\pm\frac{i}{\hbar}\int_{x_0}^{x} p(x')dx'} \tag{2.1.11}$$

We can now write the general solution, as usual we need to distinguish between two different regions:

[1]This is the reason why this is the so-called semiclassical approximation: if we perform the limit $\hbar \to 0$ we retrieve the classical mechanics, in fact also the De Broglie wavelength goes to zero.

- V(x)<E: in this region we have $p(x) \in \mathbb{R}$, so we can write $p(x) = \hbar k(x)$ with $k(x) > 0$ and the general solution is the superposition of two waves propagating in opposite directions:

$$\psi(x) = \frac{A}{\sqrt{k(x)}} e^{i \int_{x_0}^{x} k(x')dx'} + \frac{B}{\sqrt{k(x)}} e^{-i \int_{x_0}^{x} k(x')dx'} \tag{2.1.12}$$

- V(x)>E: this is the classical forbidden region, we have $p(x) \in \mathbb{C}$ so we can write $p(x) = i\hbar\tilde{k}(x)$ with $\tilde{k}(x) > 0$. The general solution reads:

$$\psi(x) = \frac{C}{\sqrt{\tilde{k}(x)}} e^{\int_{x_0}^{x} \tilde{k}(x')dx'} + \frac{D}{\sqrt{\tilde{k}(x)}} e^{-\int_{x_0}^{x} \tilde{k}(x')dx'} \tag{2.1.13}$$

2.1.1 Validity of the approximation

For the approximation to be valid, we must have the terms in $\hbar$ much smaller than the $\mathcal{O}(1)$ terms. For example, by (2.1.6), we could ask:

$$\hbar |S_0'(x) S_1'(x)| \ll |S_0'(x)|^2 \tag{2.1.14}$$

Dividing for $|S_0'(x)|$ (2.1.14) becomes $|S_1'(x)| \ll |S_0'(x)|$, if we substitute the value of $S_1'(x)$ and $S_0'(x)$ from (2.1.7a) and (2.1.7b) we find:

$$\left| \hbar \frac{p'}{p} \right| \ll |p| \,. \tag{2.1.15}$$

This condition can be read in multiples ways, dividing $\hbar$ by p we obtain:

$$\lambda(x) \left| \frac{dp}{dx} \right| \ll |p| \,. \tag{2.1.16}$$

that means that the change in the momentum over a distance equal to the de Broglie length is small compared to the momentum. Alternatively we can divide (2.1.15) by $|p|$ to obtain, after some algebra, the condition:

$$\left| \frac{d\lambda}{dx} \right| \ll 1. \tag{2.1.17}$$

Finally we can take the spatial derivative of (2.1.1), this gives us

$$|pp'| = m \left| \frac{dV(x)}{dx} \right| \tag{2.1.18}$$

and multiplying both members of (2.1.15) for $|p|$ we get:

$$\lambda(x)\left|\frac{dV(x)}{dx}\right| \ll \frac{p^2}{2m} \tag{2.1.19}$$

from which we recover the first affirmation made in this section, i.e. that WKB approximation is valid for slowly varying potential. From (2.1.17) we can easily argue that near the classical turning point, in which the potential is equal to the energy of the system, the approximation is no longer valid, since the momentum goes to zero, which implies λ increasing with no upper bound. In fact, we can approximate the potential at the left of a turning point as $V(x) - E = g(x-a)$ with $g > 0$.In the allowed region (x<a) we will have:

$$p(x)^2 = 2mg(a-x) \rightarrow \lambda(x) = \frac{2\pi\hbar}{\sqrt{2mg}\sqrt{(a-x)}} \tag{2.1.20}$$

and putting this in (2.1.17) we finally find the condition:

$$\lambda(x) = \frac{\pi\hbar}{\sqrt{2mg}(a-x)^{\frac{3}{2}}} \ll 1. \tag{2.1.21}$$

that is obviously false in the vicinity of a.

2.1.2 Connection formulae

Let's consider the solution far away from a turning point with the allowed region to the left and the forbidden region to the right. Near the turning point, we can make a linear approximation of the potential as seen before, in this way we will have in (2.1.12) and (2.1.13):

$$k^2 = \frac{2mg}{\hbar^2}(a-x) \qquad x \leq a \tag{2.1.22}$$

$$\tilde{k}^2 = \frac{2mg}{\hbar^2}(x-a) \qquad x \geq a. \tag{2.1.23}$$

In order to derive the connection formulae we are going to solve the Schrödinger equation near the turning point, with the linearized form of the potential:

$$\frac{d^2\psi}{dx^2} - \frac{2mg}{\hbar^2}(a-x) = 0 \tag{2.1.24}$$

making the substitution:

$$u = \left(\frac{2mg}{\hbar^2}\right)^{\frac{1}{3}}(x-a) \tag{2.1.25}$$

(2.1.23) becomes:

$$\frac{d^2\psi}{du^2} - u\psi = 0 \tag{2.1.26}$$

This is a well-known differential equation (see app. A), the solutions, named by his discoverer, was for the first time found by George Airy, an astronomer of the nineteenth century: $\psi(x) = aAi(u) + bBi(u)$, where:

$$Ai(u) = \frac{1}{\pi}\int_0^\infty dk \cos\big(\frac{k^3}{3} + ku\big) \tag{2.1.27}$$

and

$$Bi(u) = \frac{1}{\pi}\int_0^\infty dk \big[e^{-\frac{k^3}{3}+ku} + \sin\big(\frac{k^3}{3} + ku\big)\big]. \tag{2.1.28}$$

We can write the asymptotic form of the Airy functions as follow:

$$Ai(u) \simeq \begin{cases} \frac{1}{2}\frac{1}{\sqrt{\pi}}\,|u|^{-\frac{1}{4}}\, e^{-\frac{2}{3}|u|^{\frac{3}{2}}} & u \gg 1 \\ \frac{1}{\sqrt{\pi}}\,|u|^{-\frac{1}{4}} \cos\big(\frac{2}{3}\,|u|^{\frac{3}{2}} - \frac{\pi}{4}\big) & u \ll -1 \end{cases} \tag{2.1.29}$$

$$Bi(u) \simeq \begin{cases} \frac{1}{\sqrt{\pi}}\,|u|^{-\frac{1}{4}}\, e^{\frac{2}{3}|u|^{\frac{3}{2}}} & u \gg 1 \\ -\frac{1}{\sqrt{\pi}}\,|u|^{-\frac{1}{4}} \sin\big(\frac{2}{3}\,|u|^{\frac{3}{2}} - \frac{\pi}{4}\big) & u \ll -1 \end{cases} \tag{2.1.30}$$

We can now rewrite (2.1.12) and (2.1.13) in a more manageable way, for $x < a$:

$$\psi_L(x) = \frac{A}{\sqrt{k(x)}} \cos\left(\int_x^a k(x')dx' - \frac{\pi}{4}\right) + \frac{B}{\sqrt{k(x)}} \sin\left(\int_x^a k(x')dx' - \frac{\pi}{4}\right) \tag{2.1.31}$$

and for $x > a$:

$$\psi_R(x) = \frac{C}{\sqrt{\tilde{k}(x)}} e^{\int_a^x \tilde{k}(x')dx'} + \frac{D}{\sqrt{\tilde{k}(x)}} e^{-\int_a^x \tilde{k}(x')dx'}. \tag{2.1.32}$$

We can now express (2.1.22) and (2.1.23) in terms of u as defined in (2.1.25):

$$k = \tilde{k} = \left(\frac{2mg}{\hbar^2}\right)^{\frac{1}{3}} |u|^{\frac{1}{2}} = \eta\,|u|^{\frac{1}{2}} \tag{2.1.33}$$

and substitute these results in (2.1.31) and (2.1.32):

$$\psi_L(x) = \frac{A}{\sqrt{\eta}\,|u|^{\frac{1}{4}}} \cos\left(\frac{2}{3}\,|u|^{\frac{3}{2}} - \frac{\pi}{4}\right) + \frac{B}{\sqrt{\eta}\,|u|^{\frac{1}{4}}} \sin\left(\frac{2}{3}\,|u|^{\frac{3}{2}} - \frac{\pi}{4}\right) \tag{2.1.34}$$

$$\psi_R(x) = \frac{C}{\sqrt{\eta}\,|u|^{\frac{1}{4}}} e^{\frac{2}{3}|u|^{\frac{3}{2}}} + \frac{D}{\sqrt{\eta}\,|u|^{\frac{1}{4}}} e^{-\frac{2}{3}|u|^{\frac{3}{2}}}. \tag{2.1.35}$$

Finally we can connect the solution to the left of the turning point (2.1.34) to the solution to the right of a turning point (2.1.35) using the asymptotic form of the Airy functions in (2.1.29) and (2.1.30) finding $A = 2D$, $C = -B$ and the connection formulae:

$$\frac{2D}{\sqrt{k(x)}} \cos\left(\int_x^a k(x')dx' - \frac{\pi}{4}\right) \longleftarrow \frac{D}{\sqrt{\tilde{k}(x)}} e^{-\int_a^x \tilde{k}(x')dx'} \tag{2.1.36}$$

$$\frac{B}{\sqrt{k(x)}} \sin\left(\int_x^a k(x')dx' - \frac{\pi}{4}\right) \longrightarrow -\frac{B}{\sqrt{\tilde{k}(x)}} e^{\int_a^x \tilde{k}(x')dx'}. \tag{2.1.37}$$

The arrows are in one direction for a very precise reason: in (2.1.36) a decaying exponential to the right of the turning point implies a cosine to the left, but if we have a sine with a cosine to the left because a small error in the oscillatory function, this would imply a growing exponential to the right. In the same way, a sine to the left implies a growing exponential to the right, and even if we had a cosine together whit the sine this would implies a decaying exponential to the right that would be dominated by the growing exponential. But if we have a small error to the right, a decaying exponential, this would imply the presence of cosine to the left.

In a total analogous way, we can obtain the connection conditions for a turning point b with the forbidden region to the left and the allowed region to the right.

$$\frac{A}{\sqrt{\tilde{k}(x)}} e^{-\int_x^b \tilde{k}(x')dx'} \longrightarrow \frac{2A}{\sqrt{k(x)}} \cos\left(\int_b^x k(x')dx' - \frac{\pi}{4}\right) \tag{2.1.38}$$

$$-\frac{B}{\sqrt{\tilde{k}(x)}} e^{\int_x^b \tilde{k}(x')dx'} \longleftarrow \frac{B}{\sqrt{k(x)}} \sin\left(\int_b^x k(x')dx' - \frac{\pi}{4}\right) \tag{2.1.39}$$

2.1.3 WKB approximation for a central potential

In general the turning point is unknown, but in some cases there is a very easy way to find it. As we have already seen the radial Schrödinger equation (1.1.19) can be managed to look completely similar to the one dimensional time independent one using eq. (1.1.20), so we can apply the WKB approximation. Let's consider a potential with only a turning point, on the right of it, in order to satisfy the boundedness condition we will have only the

decaying exponential so we need to put B=0 in (2.1.31) from the connection condition (2.1.37). So for $r \ll a$ we will have:

$$\chi_L(r) = \frac{2D}{\sqrt{k(r)}} \cos\left(\int_r^a k(r')dr' - \frac{\pi}{4}\right) = \\ = \frac{2D}{\sqrt{k(r)}} \cos\left(\int_0^a k(r')dr' - \int_0^r k(r')dr' - \frac{\pi}{4}\right) \tag{2.1.40}$$

Now calling $\Delta = \int_0^a k(r')dr' - \frac{\pi}{4}$ and with some trigonometry (2.1.40) becomes:

$$\frac{2D}{\sqrt{k(r)}} \cos\left(\int_0^a k(r')dr' - \int_0^r k(x')dx' - \frac{\pi}{4}\right) = \\ = \frac{2D}{\sqrt{k(r)}} \left[\cos\left(\int_0^r k(r')dr'\right)\cos\Delta - \sin\left(\int_0^r k(r')dr'\right)\sin\Delta\right] \tag{2.1.41}$$

And from condition $\chi(0) = 0$ we obtain:

$$\frac{1}{\sqrt{k(r)}} \cos\Delta = 0 \tag{2.1.42}$$

which implies:

$$\int_0^a k(r')dr' = \big(n - \frac{1}{4}\big)\pi \quad n = 1, 2, 3 \ldots \tag{2.1.43}$$

that is a quantization condition. Exploiting the fact that $V(a) = E$ and a is unique, we can write a as a function of the energy: $a = a(E)$. Now writing the extended form of $k(x)$ we find the integral equation for the stationary state energy:

$$\int_0^{a(E)} \sqrt{\frac{2m}{\hbar^2}\big(E - V_{eff}(r')\big)}dr' = \big(n - \frac{1}{4}\big)\pi \quad n = 1, 2, 3 \ldots \tag{2.1.44}$$

2.1.4 Coulomb potential

Now we are going to test the WKB approximation on the Coulomb potential and on a linear potential, because their sum form the Cornell potential. For the sake of simplicity we solve only the cases with $l = 0$, for which can be obtained some simple formulas. We can write the Coulomb potential in a total general form:

$$V(r) = -\frac{k}{r} \tag{2.1.45}$$

with $k > 0$ and express the turning point a as a function of the energy:

$$-\frac{k}{a} = E \to a = -\frac{k}{E}. \tag{2.1.46}$$

In order to find the energy eigenvalues we need to solve (2.1.44):

$$\int_0^{-\frac{k}{E}} \sqrt{\frac{2m}{\hbar^2}\big(E + \frac{k}{r'}\big)}dr' = \big(n - \frac{1}{4}\big)\pi \quad n = 1, 2, 3\dots \tag{2.1.47}$$

let's compute the integral:

$$\int_0^{-\frac{k}{E}} \sqrt{\big(E + \frac{k}{r'}\big)}dr' = \int_0^{-\frac{k}{E}} \sqrt{\frac{Er' + k}{r'}}dr' \to r' = u^2\frac{k}{E}$$
$$\int_0^{i} \frac{\sqrt{ku^2 + k}}{u\sqrt{\frac{k}{E}}}2u\frac{k}{E}du = \int_0^{i} 2\sqrt{u^2 + 1}\frac{k}{\sqrt{E}}du.$$

Where $u \in \mathbb{C}$ and last integral is well-known and can be solved using trigonometry or hyperbolic functions, the results reads:

$$\frac{k}{\sqrt{E}}\big[x\sqrt{x^2 + 1} - \ln\big(x + \sqrt{x^2 + 1}\big)\big]\Big|_0^1 = i\frac{k}{\sqrt{E}}\frac{\pi}{2} \tag{2.1.48}$$

. If we put this result in (2.1.47) we obtain the quantization condition:

$$i\sqrt{\frac{2m}{\hbar^2}}\frac{\pi}{2}\frac{k}{\sqrt{E}} = \big(n - \frac{1}{4}\big)\pi \quad n = 1, 2, 3\dots$$
$$E = -\frac{m}{\hbar^2}\frac{8k^2}{(4n - 1)^2} \quad n = 1, 2, 3\dots \tag{2.1.49}$$

Now we can compare the theoretical results with the WKB approximation:

$$E_{th} = -\frac{m}{\hbar^2}\frac{k^2}{2n^2} \quad n = 1, 2, 3\dots \tag{2.1.50}$$

We can notice immediately that increasing n the two formulas tend to coincide (in fact the energy in WKB approximation has an asymptotic behaviour as $\frac{1}{2n^2}$). The integral in (2.1.44) cannot be easily solved in the Cornell potential case, so we have written a program to compute the energy eigenvalues for the WKB approximation: fixed n, for each value of E_i in a given range, we compute the difference:

$$\Delta E_i = \int_0^{-\frac{k}{E_i}} \sqrt{\frac{2m}{\hbar^2}\big(E_i - \frac{k}{r'}\big)}dr' - \big(n - \frac{1}{4}\big)\pi \tag{2.1.51}$$

n	E_{thSc}	E_{thWKB}	E_{numWKB}
1	-0.50000	-0.88889	-0.88889
2	-0.12500	-0.16327	-0.16327
3	-0.05556	-0.06612	-0.06612
4	-0.03125	-0.03556	-0.03556
5	-0.02000	-0.02216	-0.02216
6	-0.01389	-0.01512	-0.01512
12	-0.00347	-0.00362	-0.00362

Table 2.1.1: Coulomb potential energy eigenvalues comparison: in order from left to right the energy eigenvalues obtained from the Schrödinger equation, the ones from (2.1.49) and the ones obtained numerically.

solving the integral numerically, if $\Delta E_i \Delta E_{i+1} < 0$, the process is repeated in the range $[\Delta E_i, \Delta E_{i+1}]$ with an energy increment of $\frac{|\Delta E_i - \Delta E_{i+1}|}{10}$, in this way we can compute the energy eigenvalues with the desired number of decimal digits. In table 2.1.1 we have compared the theoretical energy eigenvalues of a Coulomb potential with $k = 1$, $c = 1$, $\hbar = 1$ and $m = 1eV$ with the energy eigenvalues obtained from (2.1.49) and the ones computed with the algorithm described above.

In figure 2.1.1 are plotted the radial eigenfunctions for the Coulomb potential with $\ell = 0$ obtained from the WKB approximation (2.1.31).

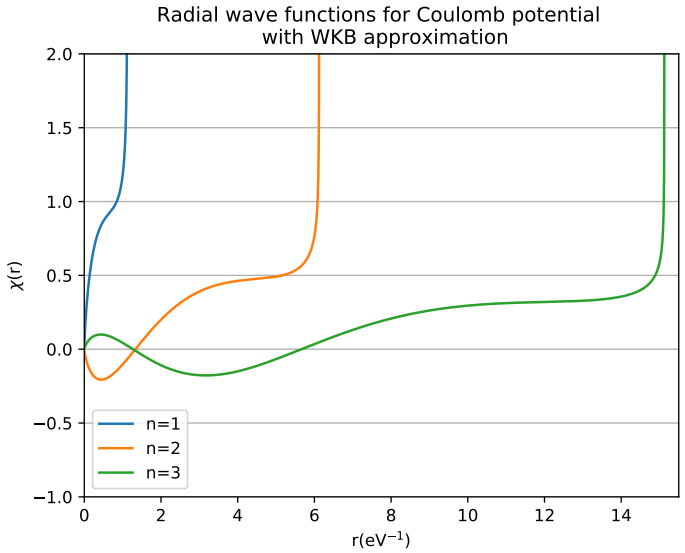

Figure 2.1.1: Radial wave functions computed with WKB approximation in the Coulomb potential case.

2.1.5 Linear potential

We want now to apply the WKB approximation to a linear potential, with $l = 0$ of the type:

$$U(r) = br. \tag{2.1.52}$$

The first thing to do is find the turning point as a function of energy

$$a = \frac{E}{b} \tag{2.1.53}$$

so we can compute the integral in (2.1.43):

$$\int_0^{\frac{E}{b}} \sqrt{\frac{2m}{\hbar^2}\big(E - br'\big)}dr' = \big(n - \frac{1}{4}\big)\pi \quad n = 1, 2, 3\ldots \tag{2.1.54}$$

that is very easy to compute and leads to the quantization equation:

$$\begin{aligned} -\sqrt{\frac{2m}{\hbar^2}}\frac{2}{3b}\big(E - br'\big)^{\frac{3}{2}}\big|_0^{\frac{E}{b}} &= \big(n - \frac{1}{4}\big)\pi \\ \sqrt{\frac{2m}{\hbar^2}}\frac{2}{3b}E^{\frac{3}{2}} &= \big(n - \frac{1}{4}\big)\pi \\ E &= \left[\frac{3b}{2}\sqrt{\frac{\hbar^2}{2m}}\big(n - \frac{1}{4}\big)\pi\right]^{\frac{2}{3}} \quad n = 1, 2, 3\ldots \end{aligned} \tag{2.1.55}$$

To compare this with the theoretical eigenvalues we have to solve the Schrödinger equation:

$$\frac{d^2\chi}{dr^2} + \frac{2m}{\hbar^2}(E - br)\chi = 0 \tag{2.1.56}$$

that we have already seen in a little different form in (2.1.24). The solution is:

$$\chi(r) = c_1\mathrm{Ai}\left(\big(\frac{2m}{\hbar^2}\big)^{\frac{1}{3}}\frac{(br - E)}{b^{\frac{2}{3}}}\right) + c_2\mathrm{Bi}\left(\big(\frac{2m}{\hbar^2}\big)^{\frac{1}{3}}\frac{(br - E)}{b^{\frac{2}{3}}}\right) \tag{2.1.57}$$

for the boundedness condition at infinity we have to impose c_2=0 and from the condition $\chi(0) = 0$ we find:

$$\mathrm{Ai}\left(-\left(\frac{2m}{b^2\hbar^2}\right)^{\frac{1}{3}}E\right) = 0. \tag{2.1.58}$$

The energy eigenvalues can be obtained from (2.1.58) with the request:

$$E = -\left(\frac{\hbar^2 b^2}{2m}\right)^{\frac{1}{3}} z_n \tag{2.1.59}$$

n	E_{thSc}	E_{thWKB}	E_{numWKB}
1	1.85576	1.84158	1.84158
2	3.24461	3.23973	3.23973
3	4.38167	4.37898	4.37898
4	5.38661	5.38483	5.38483
5	6.30526	6.30396	6.30396
6	7.16128	7.16027	7.16027
12	11.53074	11.53035	11.53035

Table 2.1.2: Linear potential energy eigenvalues comparison: in order from left to right the energy eigenvalues obtained from the Schrödinger equation, the ones from (2.1.59) and the ones obtained numerically.

where z_n is the nth zero of the Airy function Ai(x) from the right to the left. In table 2.1.2 we have compared the theoretical energy eigenvalues of a linear potential with $b = 1$, $c = 1$, $\hbar = 1$ and $m = 1eV$ with the energy eigenvalues obtained from (2.1.59) and the ones computed with the algorithm described in section 2.1.4. In figure 2.1.2 are plotted the radial eigenfunctions for the linear potential with $\ell = 0$ obtained from the WKB approximation (2.1.31).

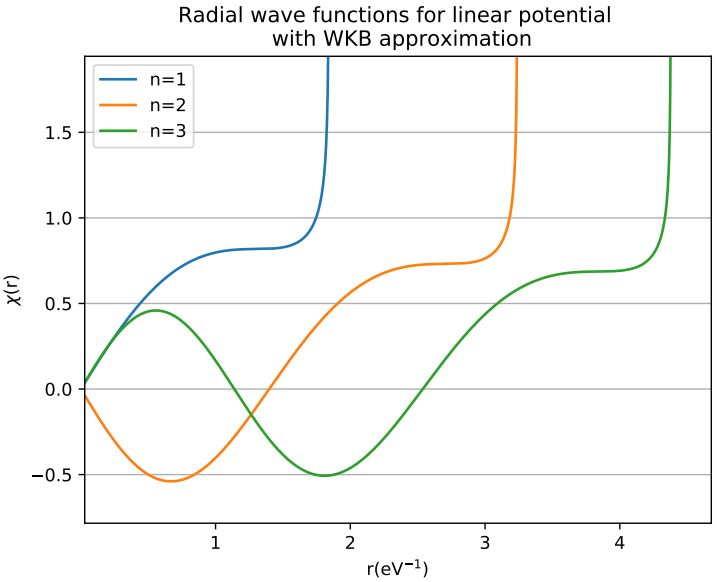

Figure 2.1.2: Radial wavefunctions computed with WKB approximation in the linear potential case.

2.2 Numerov's algorithm

The Numerov's algorithm is a method to solve numerically differential equation of the type:

$$\frac{d^2\Psi}{dx^2} = f(x)\Psi(x). \tag{2.2.1}$$

The first thing to do is to discretize the coordinate x using an uniform grid: $x_k = k\delta x$ where δx will be the algorithm step. Now we can write the Taylor expansion of $\Psi(x_{k+1}) = \Psi(x_k + \delta x)$:

$$\Psi(x_{k+1}) = \Psi(x_k) + \sum_{n=1}^{\infty} \frac{d^n\Psi}{dx^n}(x_k)\frac{\delta x^n}{n!} \tag{2.2.2}$$

and

$$\Psi(x_{k-1}) = \Psi(x_k) + \sum_{n=1}^{\infty} (-1)^n \frac{d^n\Psi}{dx^n}(x_k)\frac{\delta x^n}{n!} \tag{2.2.3}$$

From (2.2.2) and (2.2.3) follow that:

$$\Psi(x_{k+1})+\Psi(x_{k-1}) = 2\Psi(x_k)+\frac{d^2\Psi}{dx^2}(x_k)\delta x^2+\frac{1}{12}\frac{d^4\Psi}{dx^4}(x_k)\delta x^4+\mathcal{O}(\delta x^6) \tag{2.2.4}$$

We do not know the fourth derivative but we can write it using (2.2.1) and the approximation made above, neglecting the fourth order term:

$$\begin{aligned}&\frac{d^4\Psi}{dx^4}(x_k)\delta x^2 = \frac{d^2}{dx^2}\frac{d^2\Psi}{dx^2}(x_k)\delta x^2 = \frac{d^2}{dx^2}\big(f(x_k)\Psi(x_k)\big)\delta x^2 = \\ &= \Psi(x_{k+1})f(x_{k+1}) + \Psi(x_{k-1})f(x_{k-1}) - 2\Psi(x_k)f(x_k) + \mathcal{O}(\delta x^4)\end{aligned} \tag{2.2.5}$$

We can insert this approximate expression for the fourth derivative of the function in (2.2.4) which, taking in account (2.2.1), can be rewritten as follows:

$$\Psi(x_{k+1}) = \frac{2\Psi(x_k)\big(1+\frac{5}{12}f(x_k)\delta x^2\big) - \Psi(x_{k-1})\big(1-\frac{1}{12}f(x_{k-1})\delta x^2\big)}{1-\frac{1}{12}f(x_{k+1})\delta x^2} + \mathcal{O}(\delta x^6) \tag{2.2.6}$$

So if we know the first two values of the unknown function we can compute them all.

The radial Schrödinger (1.1.19) equation can be cast in the form:

$$\frac{d^2\chi}{dr^2} = \frac{2m}{\hbar^2}\big(V_{eff}(r) - E\big)\chi(r) \tag{2.2.7}$$

in which $\frac{2m}{\hbar^2}\big(V_{eff}(r)-E\big)$ plays the role of the function $f(x)$ in the Numerov's algorithm. As we have seen before, if it is valid the short distance centrifugal dominance (the potential is less singular than $\frac{1}{r^2}$ for $r \to 0$), we will have $\chi(0) = 0$, so the point from which the algorithm will begin will be $x_0 = 0$ and we will have $\chi(x_0) = \chi(0) = 0$. We now need the value of $\chi(r)$ in $x_1 = x_0 + \delta x$, because of the fact that eigenfunctions are defined up to a multiplicative constant we are free to choose any value for $\chi(x_1)$. After the function is computed we can divide it for its integral computed numerically to obtain the orthonormalized eigenfunction.

2.2.1 Finding energy eigenvalues

In equation (2.2.7) the energy eigenvalues $E_{n,l}$ are still unknown. We can find them taking into what we have seen in section 1.1. From the analysis on distribution of the energy eigenvalues we know that $E > \min(V_{eff}(r))$ and the whole discrete spectrum is contained in the interval: $\min(V_{eff}(r)) < E < V_{eff<}(r)$. In addition, for the discrete part of the spectrum, must hold the boundedness condition: $\lim_{r\to+\infty} \chi(r) = 0$. Having this information and for a fixed l we can choose an energy value E_{init} to start our research and use it to compute with the Numerov's algorithm $\chi(r, E_{init})$ with the request that $\chi(r) \to 0$ for $r \to \infty$, if this request is not satisfied we will dump this energy value and proceed with the next one, how this could be done in practice? Because reaching $r = \infty$ is impossible we have chosen a large value R of r in which the algorithm ends. Then we have made the energy varying by a fixed step ΔE and computed the product:

$$\chi(R, E) \cdot \chi(R, E + \Delta E) \tag{2.2.8}$$

if (2.2.8) it is negative this means that we have a possible energy eigenvalue between E and $E+\Delta E$. To compute accurately the jth decimal digit of E it is sufficient to repeat the algorithm described above with the energy varying in the range $[E_{j-1}, E_{j-1} + \Delta E_{j-1}]$ by a step ΔE_j, in which E_j is the energy eigenvalue with the first j decimal digits correct and $\Delta E_j = \frac{\Delta E}{10^j}$.

Reached the desired accuracy the research go over $E + \Delta E$ to find the other energy eigenvalues with the same method.

In order to verify the accuracy of the results found, we need to decrease the step δr and increase the R value, checking at which decimal digit the energy eigenvalues start to vary.

We need now to verify which energy eigenvalues we have found, to do that we count the node and apply the nodes theorem stated in the previous chapter. If $\chi(r, E_1)$ has a node in the interval $0 < r < +\infty$, E_1 is not the ground state energy and the value of E_{init} must be picked smaller.

We have written a program to perform the Numerov algorithm and find the energy eigenvalues. In appendices B and C are reported the results obtained for different values of δr and R in the Coulomb potential and the linear potential cases with our program.

Chapter 3

Determining quarkonia spectra

3.1 Determining Cornell potential parameters

3.1.1 A naive model

There are two parameters in Cornell potential(1.0.1): the strong coupling constant α_s and a.

The first one depends on the $\overline{\text{MS}}$ subtraction-scale μ, it is conventional to choose the subtraction scale of order the center of mass energy E_{CM}[4]. In our case $\mu = m_Q$, where m_Q is the quarkonium mass.

The theoretical value of α_s[5] is:

$$\alpha_s(m_Q^2) = \frac{4\pi}{\beta_0 t}\left[1 - \frac{\beta_1}{\beta_0^2}\frac{\ln t}{t} + \frac{\beta_1^2}{\beta_0^4 t^2}\left((\ln t)^2 - \ln t - 1 + \frac{\beta_2\beta_0}{\beta_1^2}\right) + \frac{\beta_1^3}{\beta_0^6 t^3}\left(-(\ln t)^3 + \frac{5}{2}(\ln t)^2 + 2\ln t - \frac{1}{2} - 3\frac{\beta_2\beta_0}{\beta_1^2}\ln t + \frac{\beta_3\beta_0^2}{\beta_1^3}\right) + \mathcal{O}\left(\frac{(\ln t)^4}{t}\right)\right] \tag{3.1.1}$$

with $t{=}\ln\dfrac{m_Q^2}{\Lambda^2}$. The β functions and Λ_{QCD} depend on the number of light

quark n_f below the energetic scale in which α_s is determined.

$$\beta_0 = 11 - \frac{2}{3}n_f \tag{3.1.2}$$

$$\beta_1 = 102 - \frac{38}{3}n_f \tag{3.1.3}$$

$$\beta_2 = \frac{2857}{2} - \frac{5033}{18}n_f + \frac{325}{54}n_f^2 \tag{3.1.4}$$

$$\beta_3 = \left(\frac{149573}{6} + 3564\zeta(3)\right) - \left(\frac{1078361}{162} + \frac{6508}{27}\zeta(3)\right)n_f + \left(\frac{50065}{162} + \frac{6472}{87}\zeta(3)\right)n_f^2 + \frac{1093}{729}n_f^3 \tag{3.1.5}$$

In order to determine the parameter a we will fit the energy spectrum predicted via Numerov method for the $b\bar{b}$ meson with the experimental one [6] that we have reported in table 3.1.1.

$n^{2s+1}L_j$	Particle name	Energy (Mev)
1^1S_0	$\eta_b(1S)$	9398.7 ± 2.0
1^3S_1	$\Upsilon(1S)$	9460.30 ± 0.26
1^1P_1	$h_b(1P)$	9899.3 ± 0.8
1^3P_0	$\chi_{b0}(1P)$	$9859.44 \pm 0.42 \pm 0.31$
1^3P_1	$\chi_{b1}(1P)$	$9892.78 \pm 0.26 \pm 0.31$
1^3P_2	$\chi_{b2}(1P)$	$9912.21 \pm 0.26 \pm 0.31$
2^3S_1	$\Upsilon(2S)$	10023.26 ± 0.31
1^3D_2	$\Upsilon_2(1D)$	10163.7 ± 1.4
2^3P_0	$\chi_{b0}(2P)$	$10232.5 \pm 0.4 \pm 0.5$
2^3P_1	$\chi_{b1}(2P)$	$10255.46 \pm 0.22 \pm 0.50$
2^3P_2	$\chi_{b2}(2P)$	$10268.65 \pm 0.22 \pm 0.50$
3^3S_1	$\Upsilon(3S)$	10355.2 ± 0.5
3^3P_1	$\chi_{b1}(3P)$	10513.4 ± 0.7
3^3P_2	$\chi_{b2}(3P)$	10524.0 ± 0.8
4^3S_1	$\Upsilon(4S)$	10579.4 ± 1.2

Table 3.1.1: The $b\bar{b}$ energy levels with spectroscopic notation known.

The $\overline{\text{MS}}$ mass of bottom quark is $m_b = 4.18\,\text{GeV}$ to which correspond a pole mass $m_{pole} = 4.78\,\text{GeV}$[6]. Using $n_f = 4$, $M_{b\bar{b}} = 2m_{pole} = 9.56\,\text{GeV}$ and $\Lambda_{QCD}^{n_f=4} = 0.292\,\text{GeV}$[7], we find $\alpha_s(M_{b\bar{b}}) = 0.177$.

Our treatment is no-relativistic, so we do not expect a splitting in energy levels due to quantum number J. On the contrary experimental data show

that this splitting exists. To overcome this difficulty, we used the mean energy value of each energetic level as the real ones that the Cornell potential should reproduce.

Finally using the list squares method we find $a = 2.76\,\mathrm{GeV}^{-1}$.

In table 3.1.2 we have written the experimentally mean energy value of each state and the ones computed via Numerov algorithm and via WKB approximation using the Cornell potential.

In this case the potential has one than more turning point on the right, if $l \neq 0$, so we have applied the WKB approximation only to S states.

As predicted by the theory the difference between the energy eigenvalue computed via WKB approximation and the ones computed via Numerov algorithm decrease as the quantum number increase.

Only for the $1P$ and $1S$ states we have all the energy experimental values for all the J values, so our calculation could be improved with more data.

nL	Exp. mean energy value	Numerov alg. predictions	WKB predictions	ΔE (MeV) th-exp
$1S$	9429.5 ± 1.13	9720.69	9610.7	291.2
$2S$	10023.26 ± 0.31	10061.06	10021.5	37.8
$3S$	10355.2 ± 0.5	10307.06	10285.8	-48.14
$4S$	10579.4 ± 1.2	10515.94	10505.2	-63.46
$1P$	$9890.93 \pm 0.44 \pm 0.31$	9965.57	-	74.46
$2P$	$10252.2 \pm 0.28 \pm 0.5$	10222.82	-	-29.38
$3P$	10518.7 ± 0.8	10438.66	-	-80.04
$1D$	10163.7 ± 1.4	10130.40	-	-33.3

Table 3.1.2: Comparison between the mean energy values and the ones predicted by Numerov algorithm and via WKB approximation

In figure 3.1.1 and 3.1.2 are drawn the normalized radial eigenfunctions computed via Numerov algorithm for the states 1S and 2S for the Coulomb potential, ($V(r) = -\frac{4}{3}\frac{\alpha_s}{r}$), the linear potential ($V(r) = \frac{r}{a^2}$) and the Cornell potential ($V(r) = -\frac{4}{3}\frac{\alpha_s}{r} + \frac{r}{a^2}$).

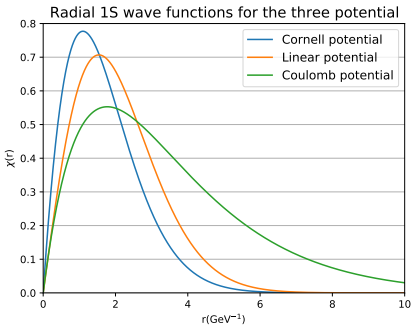

Figure 3.1.1: The normalized 1S radial wave functions for the potentials: $V(r) = -\frac{4}{3}\frac{\alpha_s}{r}$, $V(r) = \frac{r}{a^2}$ and $V(r) = -\frac{4}{3}\frac{\alpha_s}{r} + \frac{r}{a^2}$

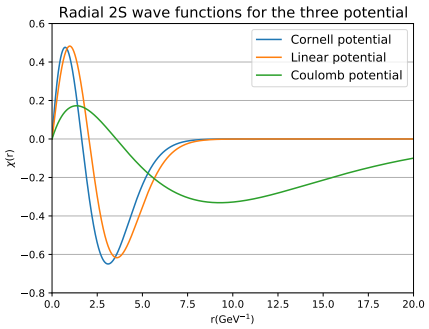

Figure 3.1.2: The normalized 2S radial wave functions for the potentials: $V(r) = -\frac{4}{3}\frac{\alpha_s}{r}$, $V(r) = \frac{r}{a^2}$ and $V(r) = -\frac{4}{3}\frac{\alpha_s}{r} + \frac{r}{a^2}$

3.1.2 Two parameters fit

Fitting only one parameter, a problem arise: all states have a positive energy eigenvalue, but experimentally 1S state has a negative energy eigenvalue.

To overcome this problem we need to increase α_s, from a physical point of view this means that the energy scale characterizing the bottomonium bound states is lower than $2m_b$ and we can extract it from the best value of α_s obtained by the two parameters fit.

The values obtained from the fit are: $\alpha_s = 0.371$ and $a = 2.39\,\mathrm{GeV}^-1$, the results of our computation are putted together in tab. 3.1.3.

nL	Exp. mean energy value	Numerov alg. predictions	WKB predictions	ΔE (MeV) th-exp
$1S$	9429.5 ± 1.13	9459.02	9160.13	29.52
$2S$	10023.26 ± 0.31	10012.96	9922.40	-10.3
$3S$	10355.2 ± 0.5	10349.00	10286.80	-6.2
$4S$	10579.4 ± 1.2	10621.31	10570.91	41.9
$1P$	$9890.93 \pm 0.44 \pm 0.31$	9916.04	-	25.74
$2P$	$10252.2 \pm 0.28 \pm 0.5$	10261.85	-	9.65
$3P$	10518.7 ± 0.8	10540.34	-	21.64
$1D$	10163.7 ± 1.4	10156.28	-	-7.42

Table 3.1.3: Comparison between the mean energy values and the ones predicted by Numerov algorithm and via WKB approximation

In figure 3.1.3 and 3.1.4 are drawn the normalized radial eigenfunctions computed via Numerov algorithm for the states 1S and 2S for the Coulomb

potential, ($V(r) = -\frac{4}{3}\frac{\alpha_s}{r}$), the linear potential ($V(r) = \frac{r}{a^2}$) and the Cornell potential ($V(r) = -\frac{4}{3}\frac{\alpha_s}{r} + \frac{r}{a^2}$).

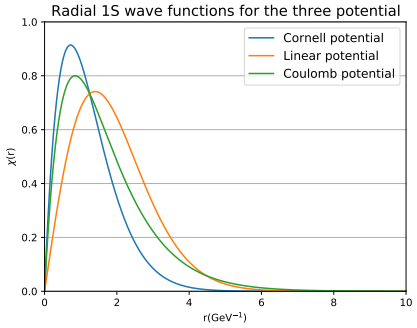

Figure 3.1.3: The normalized 1S radial wave functions for the potentials: $V(r) = -\frac{4}{3}\frac{\alpha_s}{r}$, $V(r) = \frac{r}{a^2}$ and $V(r) = -\frac{4}{3}\frac{\alpha_s}{r} + \frac{r}{a^2}$

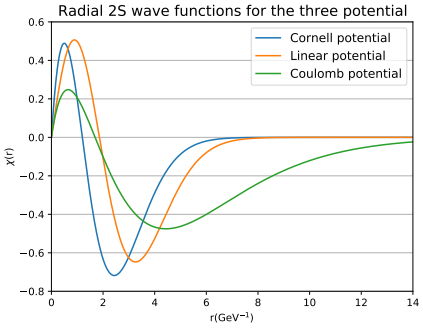

Figure 3.1.4: The normalized 2S radial wave functions for the potentials: $V(r) = -\frac{4}{3}\frac{\alpha_s}{r}$, $V(r) = \frac{r}{a^2}$ and $V(r) = -\frac{4}{3}\frac{\alpha_s}{r} + \frac{r}{a^2}$

Using (3.1.1) we can estimate the $\alpha_s(m_Q^2)$ scale, that is $m_Q \simeq 1.4\,\text{GeV}$. What is this scale?

For the first bound state we have a negative energy eigenvalue, this means that the Coulomb potential dominate the linear one, greater the mass and α_s, better this approximation become. So only for the ground state let's suppose that:

$$V_0(r) \simeq -\frac{4}{3}\frac{\alpha_s}{r} \tag{3.1.6}$$

The Schrödinger equation for this potential is analytically solvable, and the ground state energy results to be:

$$E_1 = -\frac{\mu}{2}(\frac{4}{3}\alpha_s)^2 \tag{3.1.7}$$

where μ is the mass of the quarkonium.

We can now use the virial theorem (1.1.30) which, for the Coulomb potential, lead to:

$$\langle T \rangle = -E = \frac{\mu}{2}(\frac{4}{3}\alpha_s)^2 \tag{3.1.8}$$

and because our treatment is non-relativistic, by (3.1.8) we find that:

$$v = \frac{4}{3}\alpha_s \tag{3.1.9}$$

From the hydrogen atom theory we also know that the average radius of the ground state is:

$$R_0 = \frac{3}{4\mu\alpha_s} = \frac{1}{\mu v} \tag{3.1.10}$$

in natural unit this quantity is the inverse of an energy, so we can calculate the energy scale as $\frac{1}{R_0}$, in our case this give us: $m_Q \simeq 1.18\,\mathrm{GeV}$ that is very close to the value of the energy scale obtained from (3.1.1).

These approximate calculations tell us that the energy scale in which calculate α_s is neither $2m_b$ as we have done in the previous section, neither m_b, but the one characterizing the first bound state.

3.1.3 Spin splitting

Experiments show that there is a splitting in the energy levels associated with the quantum number j. If we restrain ourselves to the S-wave functions, this effect could be taking in account in an easy way[9]. The potential for the spin-spin interaction takes the form:

$$V_{ss} = \frac{8\pi\hbar^3}{9c}\alpha_s \frac{\vec{\sigma}_q \cdot \vec{\sigma}_{\overline{q}}}{m_q m_{\overline{q}}}\delta(\vec{x}) \tag{3.1.11}$$

The expectation values of $\vec{\sigma}_q \cdot \vec{\sigma}_{\overline{q}}$ is found to be:

$$\begin{aligned}\vec{\sigma}_q \cdot \vec{\sigma}_{\overline{q}} = \frac{4}{\hbar^2}\vec{s}_q \cdot \vec{s}_{\overline{q}} = 2[S(S+1) - s_q(s_q+1) - s_{\overline{q}}(s_{\overline{q}}+1)] = \\ = \begin{cases} -3, & \text{if } S = 0 \\ +1, & \text{if } S = 1 \end{cases}\end{aligned} \tag{3.1.12}$$

where S is the total spin. The energy gap between the ${}^1S_0$ and ${}^3S_1$ levels will be:

$$\Delta E_{ss} = \frac{8\pi\hbar^3}{9c}\frac{4\alpha_s}{m_q m_{\overline{q}}}\left|\psi(0)\right|^2 \tag{3.1.13}$$

where $|\psi(0)|^2$ can be calculated, for example, using eq. (1.1.33).

Using eq. (3.1.13) we have fitted again the Bottomonium spectrum, taking into account the split in the S-levels. The best fit parameters resulted to be: $\alpha_s = 0.389$ and $a = 2.39\,\mathrm{Gev}^{-1}$, the energy obtained are reported in table 3.1.4.

The 1^1S_0 energy level it is not well predicted, this is due to the fact that the theoretical energy gap between the two $1S$ levels is about twice the experimental one.

We can repeat the calculations made in the previous paragraph about the energy scale in which α_s should be calculated. From eq. (3.1.1) we obtain $m_Q = 1.3\,\mathrm{GeV}$ and from eq. (3.1.10) $m_Q = 1.24\,\mathrm{GeV}$ with an accordance even better than before.

nL	Exp. mean energy value	Numerov alg. predictions	ΔE (MeV) th-exp
1^1S_0	9398.7 ± 2.0	9294.32	-104.4
1^3S_1	9460.30 ± 0.26	9466.72	6.42
2^3S_1	10023.26 ± 0.31	10014.41	-8.85
3^3S_1	10355.2 ± 0.5	10350.51	-4.69
4^3S_1	10579.4 ± 1.2	10623.06	43.66
$1P$	$9890.93 \pm 0.44 \pm 0.31$	9901.30	10.4
$2P$	$10252.2 \pm 0.28 \pm 0.5$	10251.12	-1.08
$3P$	10518.7 ± 0.8	10531.53	12.3
$1D$	10163.7 ± 1.4	10146.25	-17.45

Table 3.1.4: Comparison between the mean energy values and the ones predicted by Numerov algorithm with spin splitting in S-waves

3.2 Toponium spectrum

We will try now the compute toponium energy spectrum. We do not have experimental data, so we can not perform a two parameter fit as done before.

In order to estimate the strong coupling constant we need to guess the energy characterizing the first bound state. We know that α_s decreases with energy, so surely its value for the toponium case is lesser than the bottomonium one. The upper bound for the toponium first bound state energy scale will be:

$$\frac{4}{3}\alpha_s(\mathrm{b\bar{b}})\mu_{\mathrm{t\bar{t}}} \simeq 44\,\mathrm{GeV} \tag{3.2.1}$$

We know for certain that toponium reduced mass is greater than the energy characterizing the first bound state, so a lower limit for it will be:

$$\frac{4}{3}\alpha_s(\mu_{\mathrm{t\bar{t}}})\mu_{\mathrm{t\bar{t}}} \simeq 13.7\,\mathrm{GeV} \tag{3.2.2}$$

We can compute the central value of α_s using the coulombic approximation described above. (3.1.1). We know α_s should be computed at the energy scale m_Q characterizing the first bound state. From equation (3.1.10), this will be approximately:

$$m_Q = \frac{4}{3}\alpha_s(m_Q)\mu_{\mathrm{t\bar{t}}} \tag{3.2.3}$$

For each value of m_Q we can calculate the value of $\alpha_s(m_Q)$ using equation (3.1.1) until the left and right member of equation (3.2.3) are equal. Using $\Lambda_{QCD}^{n_f=5} = 0.210\,\mathrm{GeV}$, $m_{top} = 172.4\,\mathrm{GeV}$[7] we find:

$$m_Q \simeq 18\,\mathrm{GeV}$$

.

The strong coupling constant value, with this bounds, will be somewhere between $\alpha_s = 0.133$ and $\alpha_s = 0.166$, with an estimated value of $\alpha_s = 0.157$. To compute an energetic range in which we expect toponium energetic levels to be we will also allow a to vary between $a = 2.3\,\mathrm{GeV}^{-1}$ and $a = 2.5\,\mathrm{GeV}^{-1}$.

In table 3.2.1 we have reported the results of our computation.

nL	Excitation energy computed via Numerov algorithm (GeV)			Excitation energy computed via WKB approximation (GeV)		
	min	pred	max	min	pred	max
1S	−2.108342	−1.875160	−1.333800	−3.74653	−3.351237	−2.399122
1P	−0.489283	−0.425249	−0.278970			
1D	−0.154560	−0.117639	−0.038183			
1F	−0.006099	0.023964	0.082761			
2S	−0.481007	−0.415689	−0.266891	−0.651314	−0.573072	−0.387054
2P	−0.139173	−0.100151	−0.017078			
2D	0.013686	0.045950	0.107968			
2F	0.109237	0.139688	0.192635			
3S	−0.130992	−0.090722	−0.005253	−0.189138	−0.147062	−0.053077
3P	0.028493	0.062690	0.127926			
3D	0.127967	0.160424	0.216245			
3F	0.200675	0.232965	0.283890			
4S	0.036581	0.071991	0.139528	0.003290	0.038417	0.108747
4P	0.142296	0.176564	0.235336			
4D	0.218589	0.252747	0.306308			
4F	0.278834	0.313481	0.364059			
5S	0.150300	0.185753	0.246747	0.126058	0.160714	0.222794
5P	0.232524	0.268398	0.324712			
5D	0.296092	0.332502	0.385537			
5F	0.348483	0.385682	0.436762			
6S	0.240453	0.277489	0.335959	0.220662	0.256766	0.315653
6P	0.309692	0.347744	0.403375			
6D	0.365195	0.404073	0.457469			
6F	0.412151	0.451966	0.504024			

Table 3.2.1: Excitation energy for toponium calculated with Numerov algorithm and WKB approximation

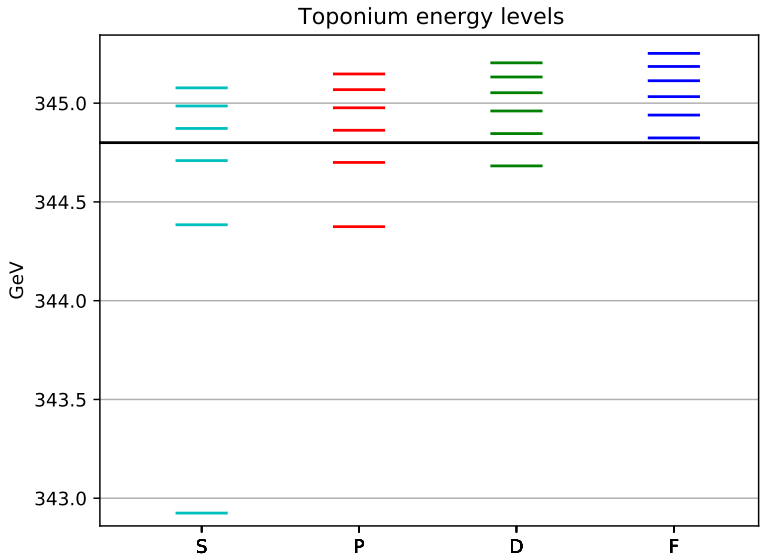

Figure 3.2.1: Expected totale energy of each toponium state.

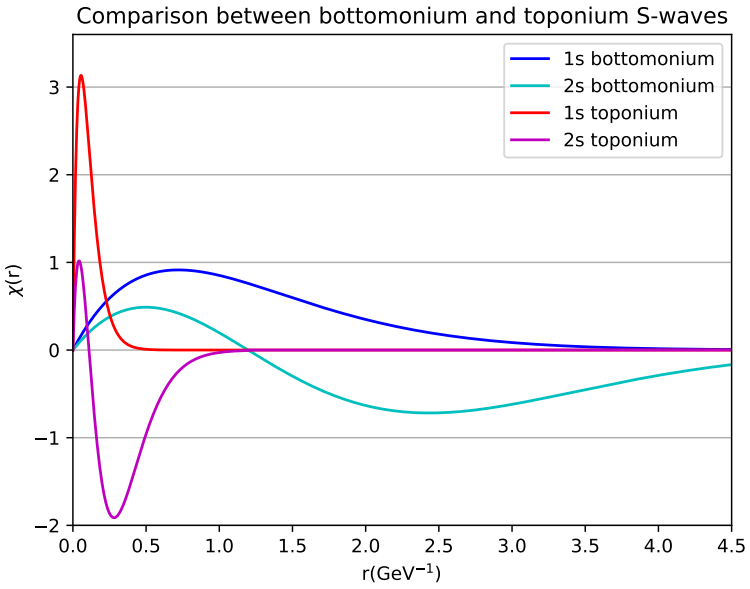

Figure 3.2.2: Comparison between $b\bar{b}$ and $t\bar{t}$ 1S and 2S wave functions.

Using eq. (3.1.13) we can compute the splitting in the S levels due to spin-spin interaction. The results are reported in tab. 3.2.2. Only for the $1S$

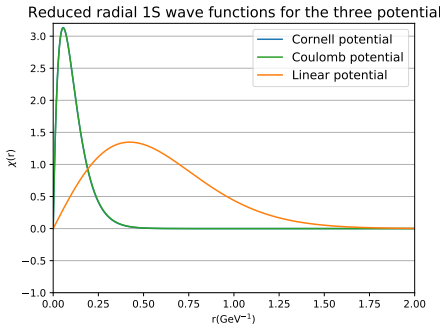

Figure 3.2.3: $1S$ normalized radial wave functions computed via Numerov algorithm for the three potential.

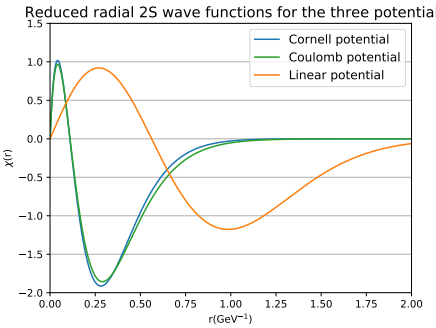

Figure 3.2.4: $2S$ normalized radial wave functions computed via Numerov algorithm for the three potential.

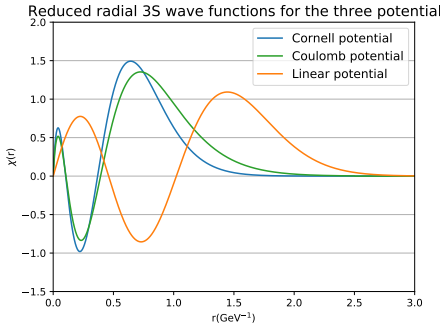

Figure 3.2.5: $3S$ normalized radial wave functions computed via Numerov algorithm for the three potential.

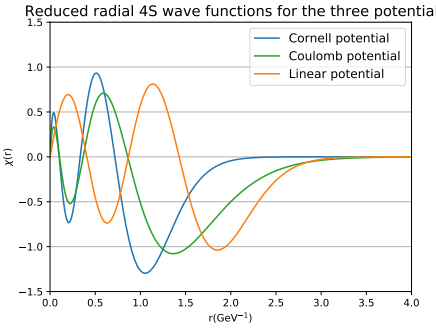

Figure 3.2.6: $4S$ normalized radial wave functions computed via Numerov algorithm for the three potential.

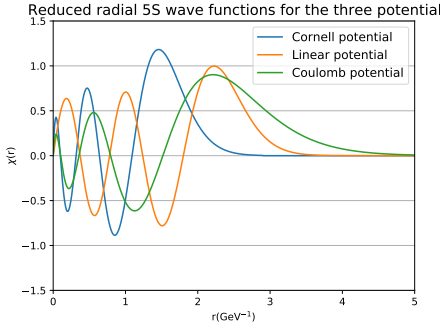

Figure 3.2.7: $5S$ normalized radial wave functions computed via Numerov algorithm for the three potential.

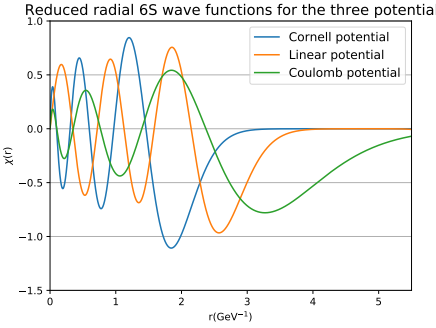

Figure 3.2.8: $6S$ normalized radial wave functions computed via Numerov algorithm for the three potential.

level the energy gap is important, being of the order of 0.1 GeV. In figure 3.2.9 are shown the new splitted S levels.

nL	E(GeV)	nL	E(GeV)
1S	-1.875160	1^1S_0	-1.958609
		1^3S_1	-1.847344
2S	-0.415689	2^1S_0	-0.427230
		2^3S_1	-0.411841
3S	-0.090722	3^1S_0	-0.095291
		3^3S_1	-0.089199
4S	0.071991	4^1S_0	0.069122
		4^3S_1	0.072947
5S	0.185753	5^1S_0	0.183552
		5^3S_1	0.186486
6S	0.277489	6^1S_0	0.275637
		6^3S_1	0.278106

Table 3.2.2: Energy eigenvalues of Cornell potential for S-waves with spin-spin splitting

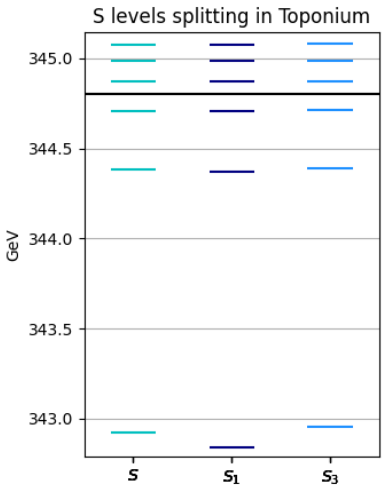

Figure 3.2.9: Total energy of S splitted levels.

Chapter 4

Constraining a new force

Let's suppose the existence of an unknown force between the top quark and the antitop quark in toponium, carried by a scalar particle of mass m. The inter-quark potential, adding Yukawa potential, would become:

$$V(r) = -\frac{4}{3}\frac{\alpha_s}{r} + \frac{r}{a^2} - G\frac{e^{-mr}}{r} \tag{4.0.1}$$

in which $G \geq 0$. We want to see what happen to the energy eigenvalues and to other relevant quantities with this hypothesis. In particular, in this section, we want to find the indicative values of G, given m, for which the variation of the 1S energy eigenvalue is greater or equal than 10%, 15% and 20%, in appendix D we have made the same calculations for other energy eigenvalues.

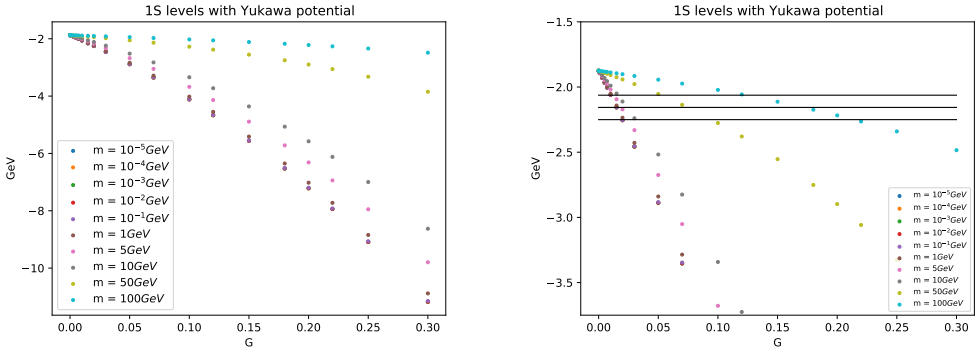

Figure 4.0.1: 1S level energy eigenvalues for different values of G and m. The black lines indicate respectively a variation from the unperturbed level of 10%, 15% and 20%.

Mass (GeV)	G value for 10% variation	G value for 15% variation	G value for 20% variation
10^{-5}	0.010	0.015	0.02
10^{-4}	0.010	0.015	0.02
10^{-3}	0.010	0.015	0.02
10^{-2}	0.010	0.015	0.02
10^{-1}	0.010	0.015	0.02
1	0.011	0.016	0.021
5	0.013	0.019	0.025
10	0.016	0.024	0.031
50	0.052	0.075	0.095
100	0.12	0.17	0.21

Table 4.0.1: Minimum value of G in function of m to obtain a percentage variation of 10%, 15%, 20% from the 1S unperturbed energy level.

4.1 Formation time and decay time

Top decays semiweakly: $t \to Wb$, we can estimate the lifetime approximately as the inverse of its width: $\Gamma_{top} = 1.42\,\text{GeV}$. Toponium is composed by a top quark and antitop one, therefore its lifetime is the half of a single top quark.

$$\tau_{lifetime} \simeq \frac{1}{2\Gamma_t} = \frac{1}{2.8\text{GeV}} \tag{4.1.1}$$

We can estimate quarkonia formation time as the revolution time of the bound state [10]. As we have already seen in the previous section, for the $1S$ state we can neglect the linear part of the Cornell potential, this is particularly true for toponium as can be seen from fig. 3.2.3 in which the coulombic eigenfunction and the Cornell one practically coincide and the difference between $E_{1SCorn} = -1.875$ and $E_{1SCoul} = -1.89$ are of the 0.8%. With a rough calculation we estimate toponium formation time, using eq. (3.1.10) and (3.1.9), as:

$$\tau_{form} \simeq \frac{2\pi r}{v} = \frac{9\pi}{8\mu\alpha_s^2} = \frac{1}{0.6\text{GeV}} \tag{4.1.2}$$

We can now make the same calculations with the new hypothetical potential. To further simplify the calculation we suppose a light mediating particle, so, if $missmall$, we can write the new potential as:

$$V(r) = -\left(\frac{4}{3}\alpha_s + G\right)\frac{1}{r} + \frac{r}{a^2} \tag{4.1.3}$$

and the formation time will decrease as:

$$\tau_{form} \simeq \frac{2\pi}{\mu(\frac{4}{3}\alpha_s + G)^2} \tag{4.1.4}$$

this allows us to estimate the minimum value of G for which the toponium could exists asking $k\tau_{form} \leq \tau_{lifetime}$ with $k \geq 1$.

$$G \geq \sqrt{k\frac{4\Gamma_t\pi}{\mu}} - \frac{4}{3}\alpha_s \tag{4.1.5}$$

Putting $k = 1$ the minimum value of G would be: $G = 0.24$.

Conclusion

Using Cornell potential we have determined some relevant quantities for toponium. We have concluded that the energy scale in which calculate α_s is about the inverse of the Bohr radius in the coulombic approximation: i.e. $m_Q \simeq \frac{4\alpha_s\mu}{3}$.

In particular for toponium this takes the value 18 GeV. 1S toponium state is characterized by an energy eigenvalue of -1.875 GeV and velocity of $\frac{4}{3}\alpha_s \simeq 0.209$.

Assuming the existence of a fifth top-philic force carried by a scalar particle, we added to Cornell potential a Yukawa one. In this way, we have established a minimum value of the intensity $G \geq 0.24$ for which it could be possible to experimentally observe toponium bounded states.

Appendix A

Airy functions

A.1 Solving the Airy equation

Airy equation reads as follow:

$$\frac{d^2u}{dx^2} - xu = 0 \tag{A.1.1}$$

In order to solve it we apply Fourier transform to both members:

$$\mathcal{F}\left(\frac{d^2u}{dx^2}\right) - \mathcal{F}(xu) = 0 \tag{A.1.2}$$

If u is sufficiently regular the following statements are true:

$$\mathcal{F}(D^a u) = (ix)^a \mathcal{F}(u) \tag{A.1.3}$$
$$\mathcal{F}(x^a u) = (iD)^a \mathcal{F}(u) \tag{A.1.4}$$
$$\overline{\mathcal{F}}\mathcal{F}u = u \tag{A.1.5}$$

Using eq. (A.1.3) and (A.1.4) in (A.1.5) we find:

$$\frac{d}{dk}\mathcal{F}(u) = ik^2\mathcal{F}(u) \tag{A.1.6}$$

that has a trivial solution:

$$\mathcal{F}(u) = Ce^{i\frac{k^3}{3}} \tag{A.1.7}$$

finally applying eq. (A.1.4) we find:

$$u(x) = \frac{C}{\sqrt{2\pi}} \int_{-\infty}^{+\infty} e^{i(\frac{k^3}{3}+kx)} dk \tag{A.1.8}$$

choosing C=$\frac{1}{\sqrt{2\pi}}$ we obtain the Airy function Ai(x).

To retrieve eq. (2.1.27) we need to work a little more:

$$\begin{aligned}
Ai(x) &= \frac{1}{2\pi}\int_{-\infty}^{\infty} e^{i(\frac{k^3}{3}+kx)}dk = \\
&= \frac{1}{2\pi}\left[\int_{-\infty}^{0} e^{i(\frac{k^3}{3}+kx)}dk + \int_{0}^{\infty} e^{i(\frac{k^3}{3}+kx)}dk\right] = \\
&= \frac{1}{2\pi}\left[\int_{0}^{\infty} e^{-i(\frac{k^3}{3}+kx)}dk + \int_{0}^{\infty} e^{i(\frac{k^3}{3}+kx)}dk\right] = \\
&= \frac{1}{\pi}\int_{0}^{\infty} \frac{e^{i(\frac{k^3}{3}+kx)} + e^{-i(\frac{k^3}{3}+kx)}}{2}dk = \\
&= \frac{1}{\pi}\int_{0}^{\infty} \cos\left(\frac{k^3}{3}+kx\right)dk
\end{aligned} \tag{A.1.9}$$

A.2 The Bi(x) function

Finding Bi(x) is more difficult. An ingenious trick is to consider k in the integral (A.1.8) a complex variable, and write Bi(x) as a sum of that integral calculated on different contours in the complex plane. Usually the contours are choose to be: $C_1 = \{k \in \mathbb{C} : \Im(k) = 0, -\infty < \Re(k) < \infty\}$ and $C_2 = \{k \in \mathbb{C} : \Im(k) = 0, -\infty < \Re(k) < 0\} \cup \{k \in \mathbb{C} : \Re(k) = 0, -\infty < \Im(k) < 0\}$.

$$\begin{aligned}
Bi(x) &= \frac{1}{2\pi}\left[-i\int_{C_1} e^{i(\frac{k^3}{3}+kx)}dk + 2i\int_{C_2} e^{i(\frac{k^3}{3}+kx)}dk\right] = \\
&= \frac{1}{2\pi}\left[-i\int_{-\infty}^{+\infty} e^{i(\frac{k^3}{3}+kx)}dk + 2i\int_{-\infty}^{0} e^{i(\frac{k^3}{3}+kx)}dk + 2i\int_{0}^{-i\infty} e^{i(\frac{k^3}{3}+kx)}dk\right] = \\
&= \frac{1}{2\pi}\left[-i\int_{0}^{\infty} e^{i(\frac{k^3}{3}+kx)} + e^{-i(\frac{k^3}{3}+kx)} + 2i\int_{0}^{+\infty} e^{-i(\frac{k^3}{3}+kx)}dk + \right. \\
&\left. + 2\int_{0}^{+\infty} e^{-\frac{k^3}{3}+kx}dk\right] = \\
&= \frac{1}{2\pi}\left[-i\int_{0}^{\infty} e^{i(\frac{k^3}{3}+kx)} - e^{-i(\frac{k^3}{3}+kx)}dk + 2\int_{0}^{+\infty} e^{-\frac{k^3}{3}+kx}dk\right] \\
&= \frac{1}{\pi}\int_{0}^{\infty} \sin\left(\frac{k^3}{3}+kx\right) + e^{-\frac{k^3}{3}+kx}dk
\end{aligned} \tag{A.2.1}$$

Appendix B

Numerov results for Coulomb potential

As usual we choose $\hbar = c = 1$ and a potential of the form:

$$V(r) = -\frac{1}{r}$$

whose theoretical energy eigenvalues are well-known (see (2.1.50)) and are written down in table B.0.1:

E_1	E_2	E_3	E_4	E_5	E_6	E_7
-0.5	-0.125	$-0.0\overline{5}$	-0.03125	-0.02	$-0.013\overline{8}$	-0.01020408

Table B.0.1: Theoretical energy eigenvalues for the Coulomb potential

In the next tables are collected the energy eigenvalues computed via Numerov's algorithm with different values of R and δr and they are compared with the theoretical prediction. If the algorithm failed in finding an energy eigenvalue in its place we have written a dash.

In table B.0.2 we have written the results for $\boldsymbol{R = 10}$:
In table B.0.3 we have written the results for $\boldsymbol{R = 50}$:
In table B.0.4 we have written the results for $\boldsymbol{R = 100}$:
In table B.0.5 we have written the results for $\boldsymbol{R = 200}$:
In table B.0.6 we have written the results for $\boldsymbol{R = 500}$:
In table B.0.7 we have written the results for $\boldsymbol{R = 1000}$:

δr Values	0.1	0.01	0.001	0.0001
E_1	−0.49701354	−0.49996627	−0.49999893	−0.49999926
E_2	−0.11228344	−0.11280046	−0.11280615	−0.11280621
E_3	–	–	–	–
E_4	–	–	–	–
E_5	–	–	–	–
E_6	–	–	–	–
E_7	–	–	–	–

Table B.0.2: Energy eigenvalues obtained for the Coulomb potential via Numerov's algorithm for $R = 50$

δr Values	0.1	0.01	0.001	0.0001
E_1	−0.49701432	−0.49996700	−0.49999967	−0.50000000
E_2	−0.12462601	−0.12499588	−0.12499996	−0.12500000
E_3	−0.05544466	−0.05555433	−0.05555554	−0.05555555
E_4	−0.03115675	−0.03120381	−0.03120433	−0.03120434
E_5	−0.01782520	−0.01786433	−0.01786476	−0.01786476
E_6	−0.00221122	−0.00226530	−0.00226590	−0.00226590
E_7	–	–	–	–

Table B.0.3: Energy eigenvalues obtained for the Coulomb potential via Numerov's algorithm for $R = 50$

δr Values	0.1	0.01	0.001	0.0001
E_1	−0.49701432	−0.49996700	−0.49999967	−0.50000000
E_2	−0.12462601	−0.12499588	−0.12499996	−0.12500000
E_3	−0.05544467	−0.05555433	−0.05555554	−0.05555556
E_4	−0.03120320	−0.03124948	−0.03124999	−0.03125000
E_5	−0.01997600	−0.01999971	−0.01999997	−0.01999997
E_6	−0.01385431	−0.01386832	−0.01386848	−0.01386848
E_7	−0.00958346	−0.00959623	−0.00959637	−0.00959637

Table B.0.4: Energy eigenvalues obtained for the Coulomb potential via Numerov's algorithm for $R = 100$

δr Values	0.1	0.01	0.001	0.0001
E_1	−0.49701432	−0.49996700	−0.49999967	−0.50000000
E_2	−0.12462601	−0.12499588	−0.12499996	−0.12500000
E_3	−0.05544467	−0.05555433	−0.05555554	−0.05555556
E_4	−0.03120320	−0.03124948	−0.03124999	−0.03125000
E_5	−0.01997603	−0.01999974	−0.02000000	−0.02000000
E_6	−0.01387502	−0.01388874	−0.01388889	−0.01388889
E_7	−0.01019535	−0.01020399	−0.01020408	−0.01020408

Table B.0.5: Energy eigenvalues obtained for the Coulomb potential via Numerov's algorithm for $R = 200$

δr Values	0.1	0.01	0.001	0.0001
E_1	−0.49701432	−0.49996700	−0.49999967	−0.50000000
E_2	−0.12462601	−0.12499588	−0.12499996	−0.12500000
E_3	−0.05544467	−0.05555433	−0.05555554	−0.05555556
E_4	−0.03120320	−0.03124948	−0.03124999	−0.03125000
E_5	−0.01997603	−0.01999974	−0.02000000	−0.02000000
E_6	−0.01387502	−0.01388874	−0.01388889	−0.01388889
E_7	−0.01019535	−0.01020399	−0.01020408	−0.01020408

Table B.0.6: Energy eigenvalues obtained for the Coulomb potential via Numerov's algorithm for $R = 500$

δr Values	0.1	0.01	0.001	0.0001
E_1	-0.49701432	-0.49996700	-0.49999967	-0.50000000
E_2	-0.12462601	-0.12499588	-0.12499996	-0.12500000
E_3	-0.05544467	-0.05555433	-0.05555554	-0.05555556
E_4	-0.03120320	-0.03124948	-0.03124999	-0.03125000
E_5	-0.01997603	-0.01999974	-0.02000000	-0.02000000
E_6	-0.01387502	-0.01388874	-0.01388889	-0.01388889
E_7	-0.01019535	-0.01020399	-0.01020408	-0.01020408

Table B.0.7: Energy eigenvalues obtained for the Coulomb potential via Numerov's algorithm for $R = 1000$

Appendix C

Numerov results for linear potential

As usual we choose $\hbar = c = 1$ and a potential of the form: $V(r) = r$ whose theoretical energy eigenvalues are well-known (see (2.1.59)) and are written down in table C.0.1:

E_1	1.85575708
E_2	3.24460762
E_3	4.38167124
E_4	5.38661378
E_5	6.30526301
E_6	7.16128273
E_7	7.96889166

Table C.0.1: Theoretical energy eigenvalues for a linear potential.

In the next tables are collected the energy eigenvalues computed via Numerov's algorithm with different values of R and δr.

In table C.0.2 we have written the results for $\boldsymbol{R = 10}$:

In table C.0.3 we have written the results for $\boldsymbol{R = 50}$:

In table C.0.4 we have written the results for $\boldsymbol{R = 100}$:

δr Values	0.1	0.01	0.001	0.0001
E_1	1.85575676	1.85575708	1.85575708	1.85575708
E_2	3.24460068	3.24460762	3.24460763	3.24460763
E_3	4.38165236	4.38167124	4.38167124	4.38167124
E_4	5.38657765	5.38661378	5.38661378	5.38661378
E_5	6.30520451	6.30526321	6.30526322	6.30526322
E_6	7.16121161	7.16129822	7.16129823	7.16129823
E_7	7.96927727	7.9693974	7.96939741	7.96939741

Table C.0.2: Energy eigenvalues obtained for the linear potential via Numerov's algorithm for $R = 10$.

δr Values	0.1	0.01	0.001	0.0001
E_1	1.85575676	1.85575708	1.85575708	1.85575708
E_2	3.24460068	3.24460762	3.24460763	3.24460763
E_3	4.38165236	4.38167124	4.38167124	4.38167124
E_4	5.38657765	5.38661378	5.38661378	5.38661378
E_5	6.30520430	6.30526300	6.30526301	6.30526301
E_6	7.16119611	7.16128272	7.16128273	7.16128273
E_7	7.96877179	7.96889164	7.96889166	7.96889166

Table C.0.3: Energy eigenvalues obtained for the linear potential via Numerov's algorithm for $R = 50$.

δr Values	0.1	0.01	0.001	0.0001
E_1	1.85575676	1.85575708	1.85575708	1.85575708
E_2	3.24460068	3.24460762	3.24460763	3.24460763
E_3	4.38165236	4.38167124	4.38167124	4.38167124
E_4	5.38657765	5.38661378	5.38661378	5.38661378
E_5	6.30520430	6.30526300	6.30526301	6.30526301
E_6	7.16119611	7.16128272	7.16128273	7.16128273
E_7	7.96877179	7.96889164	7.96889166	7.96889166

Table C.0.4: Energy eigenvalues obtained for the linear potential via Numerov's algorithm for $R = 100$.

Appendix D

Variations in toponium energy levels due to Yukawa potential

In this appendix are reported the energy eigenvalues of the Schrödinger equation with the potential (4.0.1). We have considered the levels that unperturbed have a negative energy eigenvalue and the first ones for each value of l that have a positive energy eigenvalue.

Mass (GeV)	G value for 10% variation	G value for 15% variation	G value for 20% variation
10^{-5}	0.009	0.013	0.017
10^{-4}	0.009	0.013	0.017
10^{-3}	0.009	0.013	0.017
10^{-2}	0.009	0.013	0.017
10^{-1}	0.009	0.013	0.017
1	0.01	0.015	0.02
5	0.019	0.027	0.036
10	0.029	0.042	0.056
50	0.092	0.13	0.17
100	0.2	0.27	0.34

Table D.0.1: Minimum value of G in function of m to obtain a percentage variation of 10%, 15%, 20% from the 2S unperturbed energy level.

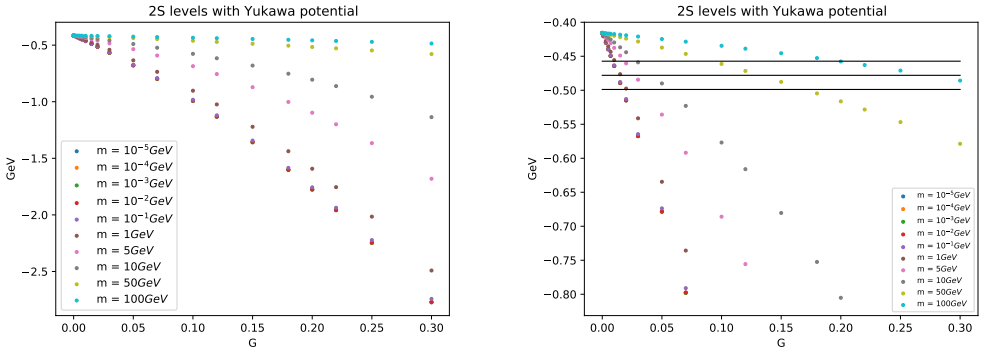

Figure D.0.1: 2S level energy eigenvalues for different values of G and m. The black lines indicate respectively a variation from the unperturbed level of 10%, 15% and 20%.

Mass (GeV)	G value for 10% variation	G value for 15% variation	G value for 20% variation
10^{-5}	0.004	0.006	0.007
10^{-4}	0.004	0.006	0.007
10^{-3}	0.004	0.006	0.007
10^{-2}	0.004	0.006	0.007
10^{-1}	0.004	0.006	0.008
1	0.005	0.008	0.01
5	0.012	0.017	0.023
10	0.018	0.026	0.035
50	0.055	0.08	0.11
100	0.12	0.17	0.22

Table D.0.2: Minimum value of G in function of m to obtain a percentage variation of 10%, 15%, 20% from the 3S unperturbed energy level.

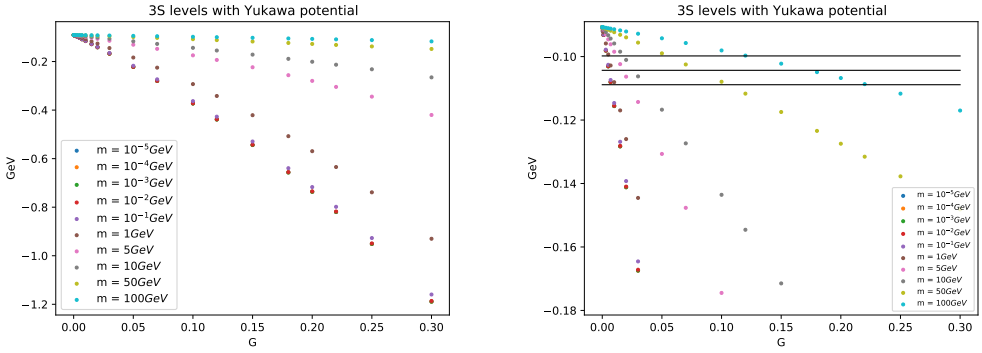

Figure D.0.2: 3S level energy eigenvalues for different values of G and m. The black lines indicate respectively a variation from the unperturbed level of 10%, 15% and 20%.

Mass (GeV)	G value for 10% variation	G value for 15% variation	G value for 20% variation
10^{-5}	0.004	0.006	0.008
10^{-4}	0.004	0.006	0.008
10^{-3}	0.004	0.006	0.008
10^{-2}	0.004	0.006	0.008
10^{-1}	0.004	0.007	0.009
1	0.007	0.01	0.014
5	0.016	0.024	0.031
10	0.023	0.034	0.046
50	0.069	0.1	0.13
100	0.15	0.22	0.27

Table D.0.3: Minimum value of G in function of m to obtain a percentage variation of 10%, 15%, 20% from the 4S unperturbed energy level.

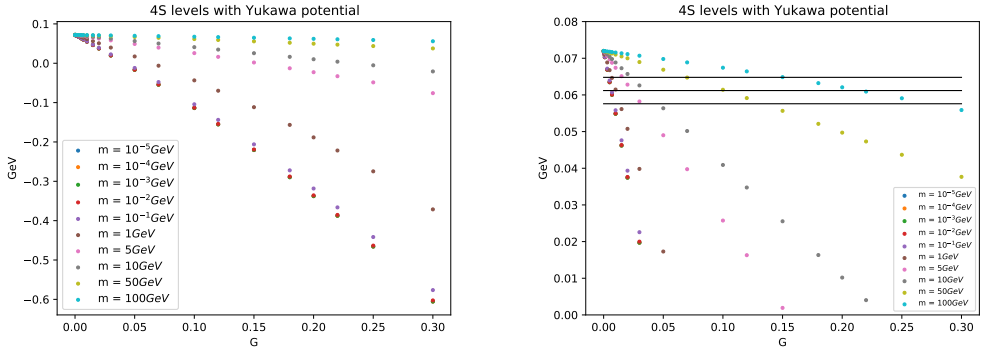

Figure D.0.3: 4S level energy eigenvalues for different values of G and m. The black lines indicate respectively a variation from the unperturbed level of 10%, 15% and 20%.

Mass (GeV)	G value for 10% variation	G value for 15% variation	G value for 20% variation
10^{-5}	0.009	0.013	0.017
10^{-4}	0.009	0.013	0.017
10^{-3}	0.009	0.013	0.017
10^{-2}	0.009	0.013	0.017
10^{-1}	0.009	0.013	0.018
1	0.011	0.016	0.021
5	0.022	0.032	0.041
10	0.045	0.064	0.081
50	> 0.3	> 0.3	> 0.3
100	> 0.3	> 0.3	> 0.3

Table D.0.4: Minimum value of G in function of m to obtain a percentage variation of 10%, 15%, 20% from the 1P unperturbed energy level.

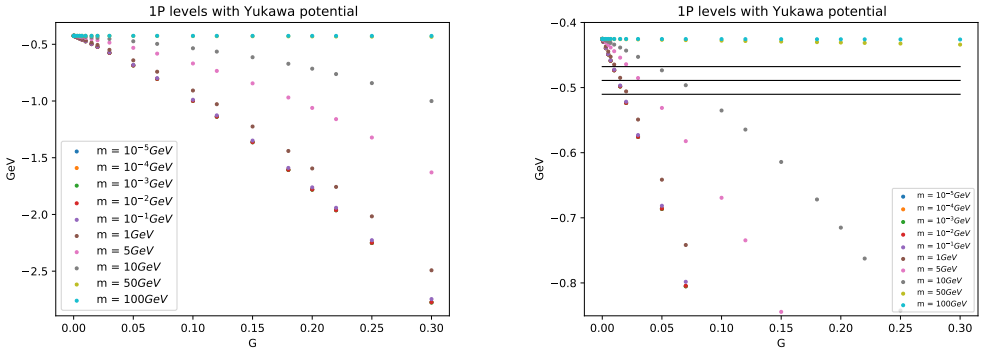

Figure D.0.4: 1P level energy eigenvalues for different values of G and m. The black lines indicate respectively a variation from the unperturbed level of 10%, 15% and 20%.

Mass (GeV)	G value for 10% variation	G value for 15% variation	G value for 20% variation
10^{-5}	0.004	0.006	0.008
10^{-4}	0.004	0.006	0.008
10^{-3}	0.004	0.006	0.008
10^{-2}	0.004	0.006	0.008
10^{-1}	0.004	0.006	0.009
1	0.006	0.009	0.012
5	0.016	0.024	0.032
10	0.033	0.048	0.063
50	> 0.3	> 0.3	> 0.3
100	> 0.3	> 0.3	> 0.3

Table D.0.5: Minimum value of G in function of m to obtain a percentage variation of 10%, 15%, 20% from the 2P unperturbed energy level.

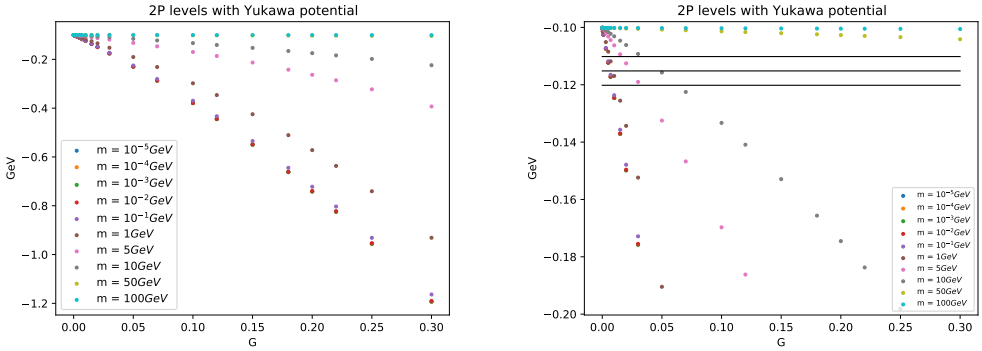

Figure D.0.5: 2P level energy eigenvalues for different values of G and m. The black lines indicate respectively a variation from the unperturbed level of 10%, 15% and 20%.

Mass (GeV)	G value for 10% variation	G value for 15% variation	G value for 20% variation
10^{-5}	0.004	0.006	0.008
10^{-4}	0.004	0.006	0.008
10^{-3}	0.004	0.006	0.008
10^{-2}	0.004	0.006	0.008
10^{-1}	0.004	0.006	0.008
1	0.006	0.009	0.013
5	0.018	0.027	0.035
10	0.035	0.051	0.067
50	> 0.3	> 0.3	> 0.3
100	> 0.3	> 0.3	> 0.3

Table D.0.6: Minimum value of G in function of m to obtain a percentage variation of 10%, 15%, 20% from the 3P unperturbed energy level.

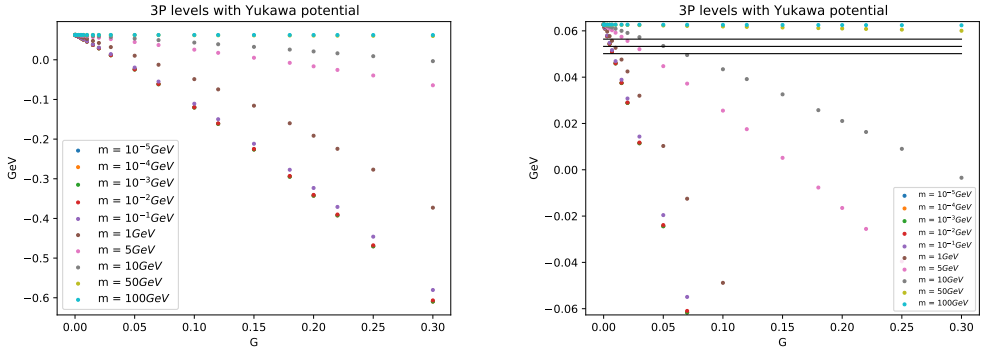

Figure D.0.6: 3P level energy eigenvalues for different values of G and m. The black lines indicate respectively a variation from the unperturbed level of 10%, 15% and 20%.

Mass (GeV)	G value for 10% variation	G value for 15% variation	G value for 20% variation
10^{-5}	0.005	0.007	0.01
10^{-4}	0.005	0.007	0.01
10^{-3}	0.005	0.007	0.01
10^{-2}	0.005	0.007	0.01
10^{-1}	0.005	0.008	0.01
1	0.007	0.011	0.015
5	0.03	0.044	0.057
10	0.12	0.17	0.21
50	> 0.3	> 0.3	> 0.3
100	> 0.3	> 0.3	> 0.3

Table D.0.7: Minimum value of G in function of m to obtain a percentage variation of 10%, 15%, 20% from the 1D unperturbed energy level.

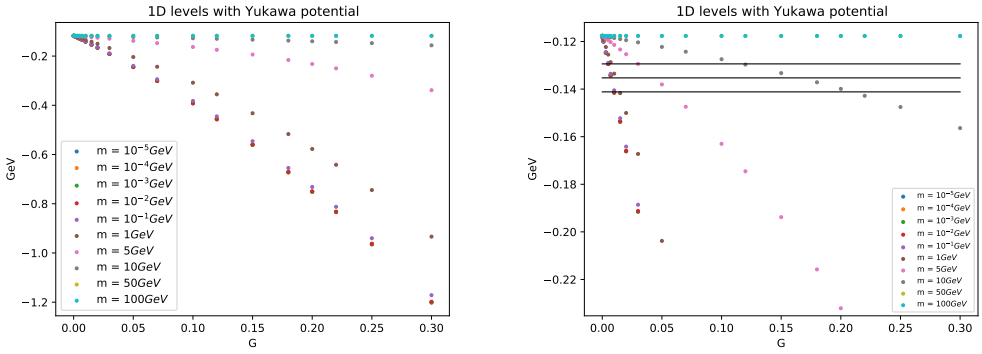

Figure D.0.7: 1D level energy eigenvalues for different values of G and m. The black lines indicate respectively a variation from the unperturbed level of 10%, 15% and 20%.

Mass (GeV)	G value for 10% variation	G value for 15% variation	G value for 20% variation
10^{-5}	0.003	0.004	0.006
10^{-4}	0.003	0.004	0.006
10^{-3}	0.003	0.004	0.006
10^{-2}	0.003	0.004	0.006
10^{-1}	0.003	0.005	0.006
1	0.005	0.008	0.01
5	0.022	0.032	0.042
10	0.072	0.11	0.14
50	> 0.3	> 0.3	> 0.3
100	> 0.3	> 0.3	> 0.3

Table D.0.8: Minimum value of G in function of m to obtain a percentage variation of 10%, 15%, 20% from the 2D unperturbed energy level.

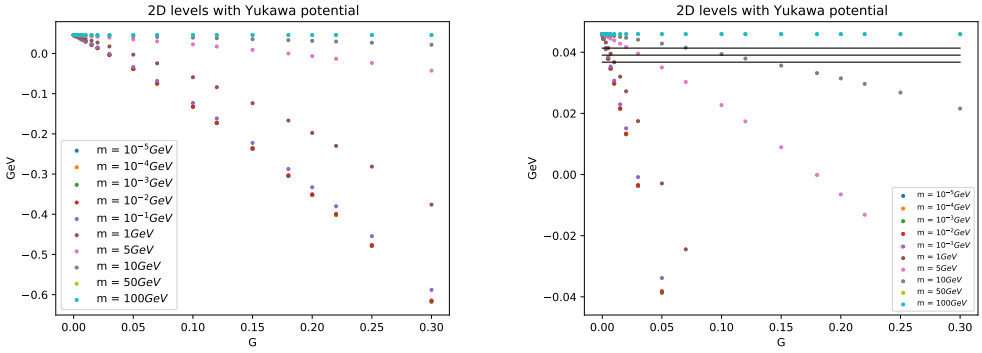

Figure D.0.8: 2D level energy eigenvalues for different values of G and m. The black lines indicate respectively a variation from the unperturbed level of 10%, 15% and 20%.

Mass (GeV)	G value for 10% variation	G value for 15% variation	G value for 20% variation
10^{-5}	0.0015	0.0025	0.003
10^{-4}	0.0015	0.0025	0.003
10^{-3}	0.0015	0.0025	0.003
10^{-2}	0.0015	0.0025	0.003
10^{-1}	0.0015	0.0025	0.0035
1	0.003	0.0045	0.055
5	0.024	0.036	0.048
10	0.2	0.28	0.37
50	> 0.3	> 0.3	> 0.3
100	> 0.3	> 0.3	> 0.3

Table D.0.9: Minimum value of G in function of m to obtain a percentage variation of 10%, 15%, 20% from the 1F unperturbed energy level.

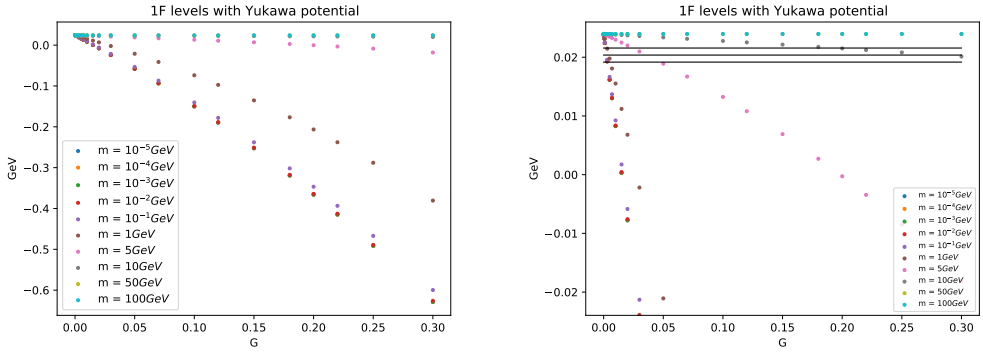

Figure D.0.9: 1F level energy eigenvalues for different values of G and m. The black lines indicate respectively a variation from the unperturbed level of 10%, 15% and 20%.

Bibliography

[1] C. Quigg, J. L. Rosner, "Quantum Mechanics with Applications to Quarkonium", FERMILAB-Pub-79/22-THY February 1979

[2] E. Eichten, K. Gottfried, T. Kinoshita, K. D. Lane, T. M. Yan, "Charmonium: The model", Physical Review D, Volume 17, Number 11, 1 June 1978

[3] *Barton Zwiebach's Lecture Notes*, 8.06 Quantum Physics III. Spring 2018. Massachusetts Institute of Technology.

[4] Hinchliffe, Ian, and Aneesh Manohar. "The QCD Coupling Constant." Annual Review of Nuclear and Particle Science 50.1 (2000): 643–678.

[5] Deur, Alexandre, Stanley J. Brodsky, and Guy F. de Téramond. "The QCD Running Coupling." Progress in Particle and Nuclear Physics 90 (2016): 1–74.

[6] P.A. Zyla et al. (Particle Data Group), Prog. Theor. Exp. Phys. 2020, 083C01 (2020)

[7] https://pdg.lbl.gov/2018/reviews/rpp2018-rev-qcd.pdf

[8] N. Brambilla, X. Garcia i Tormo, J. Soto and A. Vairo, Extraction of α_s from radiative $\Upsilon(1S)$ decays, Phys. Rev. D 75, 074014 (2007) [hep-ph/0702079]

[9] Povh, B., Rith, K., Scholz, C., Zetsche, F., Rodejohann, W, "Particles and nuclei - An Introduction to the Physical Concepts", Springer, 2015

[10] I.I.Y. Bigi, Y.L. Dokshitzer, V.A. Khoze, J.H. Kühn, P.M. Zerwas, "Production and decay properties of ultra-heavy quarks" Phys. Lett. B 181, 157 (1986)